Acta Mechanica Solida Sinica (2023) 36:361–389
https://doi.org/10.1007/s10338-023-00383-2

Review on the Theories and Applications of Dynamic Condensation and Component Mode Synthesis Methods in Solving FEM-based Structural Dynamics

Yuhan Sun[1] · Yu Lu[1] · Zhiguang Song[1]

Received: 9 October 2022 / Revised: 5 February 2023 / Accepted: 6 February 2023 / Published online: 12 April 2023

Abstract
The rapid development of modern science, technology, and industrialization has promoted the birth of more large and complex engineering structures. When the finite element (FE) method is used for dynamic analysis of these structures, such as high-rise buildings, aircraft, and ships, the structural FE models often contain millions of degrees of freedom. This will lead to great hardware and computing costs, which is often unacceptable in the engineering field. Therefore, many FE model reduction technologies have been developed, among which dynamic condensation and component mode synthesis are the most widely used methods. This paper reviews the historical processes and general theoretical framework of these two main categories of FE model reduction technologies and briefly summarizes the latest applications of these methods in the engineering field. Current bottlenecks in dynamic condensation and component mode synthesis methods, as well as solutions found in literature, are also briefly discussed. Finally, this paper gives a conclusion and brief prospects for future research. This review aims to comprehensively introduce the two most widely used methods of FE model reduction technologies and hopes to provide suggestions and guidance for developing new model reduction technologies.

Keywords FEM · Structural dynamics · Dynamic condensation · Component mode synthesis

Abbreviations

FEM	Finite element method
SFE	Stochastic finite element
SFEM	Stochastic finite element method
WFEM	Wave and finite element method
DC	Dynamic condensation
CMS	Component mode synthesis
DOFs	Degrees of freedom
P–C	Polynomial chaos
FGM	Functionally graded materials
NSEMR-II	Neumann series expansion-based second-order model reduction
IRS	Improved reduced system method
IIRS	Iterated improved reduced system method
DIRS	Dynamic improved reduced system method
IOR	Iterative order reduction method
SEREP	System equivalent reduction expansion process
C-B	Craig-Bampton method
ECB	Enhanced Craig-Bampton method
B-H	Benfield-Hruda method
MD	Mode displacement method
MA	Mode acceleration method
MTA	Modal truncation augmentation method
COC	Cross-orthogonality checks
MAC	Modal assurance criterion
MCS	Monte Carlo simulation
ERMT	Equivalent reduced model technique
BIW	Body-in-white
ANN	Artificial neural network
CDLA	Coupled dynamic loads analysis
ROMs	Reduced order models
FRF	Frequency response function

Yuhan Sun and Yu Lu contributed equally to this work and should be considered as co-first authors.

✉ Zhiguang Song
z.g.song@hrbeu.edu.cn

[1] College of Aerospace and Civil Engineering, Harbin Engineering University, Harbin 150001, China

S-CC mode	System-level characteristic constraint mode
L-CC mode	Local-level characteristic constraint mode
CFD	Computational fluid dynamics

1 Introduction

The FEM is a numerical calculation method proposed and developed in recent decades. The idea of this method is to discretize the continuous structure into an aggregate of finite elements and nodes for analysis and transform the analysis of infinite unknowns into the analysis of finite unknowns. The FEM is suitable for the analysis of many kinds of problems such as statics, dynamics, and multi-physical field coupling, and therefore widely used in various engineering fields. However, for the analysis of large and complex structures such as cars, aircraft, ships, buildings, and other engineering structures [1–3], due to the large number of elements, the calculation time can be very long. In addition, the requirements of computational server are particularly high for structures that require multiple-feedback iterative optimization. For example, Fan et al. [4] established a fine finite element model of a shaking table. The model was meshed by 8-node hexahedral elements with about 20,000,000 DOFs. The calculation was carried out on a YH supercomputer that includes thousands of blade computing nodes which contain 12 Intel processors and 48 GB of shared memory. It took about 20,700 s to calculate the first 100 characteristic values of the structure. Fan et al. [5] updated the FE model of the SGIII prototype laser facility, making its DOFs reach 154,171,842, and spent 92,868 s to calculate the first 100 order modes of the structure through parallel calculation using 2,048 processors. At present, large fine finite element models [6, 7] are ubiquitous in engineering fields. The large amount of time and hardware costs has become the biggest challenge for FEM applications.

In order to obtain reduced finite element models, the dynamic condensation and component mode synthesis (CMS) methods have been proposed. Dynamic condensation methods are mainly divided into the Guyan reduction method [8], the Kidder method [9], the improved reduction system (IRS) method [10], and the system equivalent reduction expansion process (SEREP) method [11], while CMS methods are mainly divided into the fixed interface component mode synthesis method [12], the free interface component mode synthesis method [13], and the mixed interface component mode synthesis method [14].

The significant difference between dynamic condensation and CMS is that the dynamic condensation technology reduces the FE model in the physical space, while the CMS method completes this work in the modal space [15]. Therefore, they have been applied in different engineering fields. In particular, dynamic condensation is specialized for experiment and FE analysis correlation, virtual sensing, and iterative updating of the FE model [16–19]. CMS, as its name implies, is a model reduction technology for components or substructures. Taking the aircraft production as an example to illustrate the concept of the substructure, aircraft components such as the nose, fuselage, and wings can be designed and produced by different production teams before final assembly. These components are called substructures in product design and analysis. When the entire aircraft structure needs to be analyzed, only the FE model of the substructure established by each development team needs to be integrated, which benefits the information security between the development teams. In addition, when a single substructure needs frequent design modifications, the CMS method has unique advantages [15]. The concept of substructure is a key feature of the CMS method. Therefore, the CMS method is widely used in the analysis, design, and production of aircraft, vehicles, satellites, and other structures.

In recent decades, dynamic condensation and CMS methods have been widely used in various engineering fields to obtain reduced finite element models. This paper aims to review the two finite element model reduction techniques through three aspects, i.e., the historical process, general theoretical framework, and latest applications. At the end of this paper, the problems and solutions of the two model reduction technologies are summarized, and the future development is prospected.

2 FE Model Reduction Techniques

Considering a dynamic problem, the FE equation of motion without damping is

$$\boldsymbol{M}\ddot{\boldsymbol{u}} + \boldsymbol{K}\boldsymbol{u} = \boldsymbol{F} \tag{1}$$

where $\boldsymbol{M}$ and $\boldsymbol{K}$ are the structural mass and stiffness matrices, and $\boldsymbol{u}$ and $\boldsymbol{F}$ are the vectors of generalized coordinates and external loads, respectively. It is worth mentioning that the following reduction techniques are also applicable to the calculation of the proportional damping system. The problem of the non-classical damping (non-proportional damping) vibration system will be further discussed later. There are various methods that can be employed to reduce the size of the FE model and produce the transformation matrix.

2.1 Dynamic Condensation

$\boldsymbol{M} \in \mathbf{R}^{N\times N}$ and $\boldsymbol{K} \in \mathbf{R}^{N\times N}$ are positive or semi-positive definite matrices, where N is the number of degrees of freedom

(DOFs) in the original model. In the dynamic condensation, a small proportion of the dominant DOFs, known as "master DOFs", are retained in the reduced model, while the remaining DOFs, known as "slave DOFs", are eliminated. Generally, the number of master DOFs, N_m, is much smaller than the total DOFs, that is, $N_m << N$. Therefore, when the slave DOFs are eliminated, the size of the original model can be significantly reduced. In Eq. (1), the stiffness matrix, mass matrix, displacement vector, and force vector can be divided into blocks according to the master and slave DOFs. It should be emphasized that the DOFs of the nodes subjected to external load are generally selected as the master DOFs. The specific selection criteria of the master DOFs will be discussed in detail in Sect. 3.1. Therefore, it is assumed that the external load acting on the slave DOFs is zero,

$$\begin{bmatrix} \boldsymbol{M}_{mm} & \boldsymbol{M}_{ms} \\ \boldsymbol{M}_{sm} & \boldsymbol{M}_{ss} \end{bmatrix} \begin{Bmatrix} \ddot{\boldsymbol{u}}_m \\ \ddot{\boldsymbol{u}}_s \end{Bmatrix} + \begin{bmatrix} \boldsymbol{K}_{mm} & \boldsymbol{K}_{ms} \\ \boldsymbol{K}_{sm} & \boldsymbol{K}_{ss} \end{bmatrix} \begin{Bmatrix} \boldsymbol{u}_m \\ \boldsymbol{u}_s \end{Bmatrix} = \begin{Bmatrix} \boldsymbol{F}_m \\ \boldsymbol{0} \end{Bmatrix} \tag{2}$$

where the subscripts "m" and "s" denote the master and slave, respectively.

2.1.1 The Guyan Reduction

In the 1960s, Guyan [8], as a pioneer in the field of reduction technology, proposed the well-known Guyan reduction method. Almost at the same time, similar methods were introduced by Irons [20, 21] and is generally referred to as static reduction (sometimes also referred to as the Irons-Guyan reduction, eigenvalue economizer, or mass condensation). In addition, Guyan reduction is also the first dynamic condensation method that provides other scholars with an important idea of model reduction. Since then, various new dynamic condensation methods have been proposed [9–11, 22, 23].

The basis of Guyan reduction may follow the procedure used in Ref. [24] for the stiffness matrix. The vector of slave DOFs $\boldsymbol{u}_s$ can be expressed in terms of the master DOFs $\boldsymbol{u}_m$ as

$$\boldsymbol{u}_s = -\boldsymbol{K}_{ss}^{-1}\boldsymbol{K}_{sm}\boldsymbol{u}_m \tag{3}$$

As a result, the total DOFs $\boldsymbol{u}$ can now be approximated as

$$\boldsymbol{u} = \begin{Bmatrix} \boldsymbol{u}_m \\ \boldsymbol{u}_s \end{Bmatrix} = \begin{Bmatrix} \boldsymbol{I} \\ -\boldsymbol{K}_{ss}^{-1}\boldsymbol{K}_{sm} \end{Bmatrix} \boldsymbol{u}_m = \boldsymbol{T}_G\boldsymbol{u}_m \tag{4}$$

where $\boldsymbol{T}_G$ is the coordinate transformation matrix of Guyan reduction. Actually, the transformation matrix is used to transform the space of total DOFs to the master DOFs, and during this transformation, the DOFs is significantly reduced. As a result, following the method of coordinate transformation, the reduced mass and stiffness matrices are given by

$$\begin{aligned} \boldsymbol{M}_G = \boldsymbol{T}_G^{\mathrm{T}}\boldsymbol{M}\boldsymbol{T}_G = \boldsymbol{M}_{mm} - \boldsymbol{K}_{ms}\boldsymbol{K}_{ss}^{-1}\boldsymbol{M}_{sm} \\ - \boldsymbol{M}_{ms}\boldsymbol{K}_{ss}^{-1}\mathbf{K}_{sm} + \boldsymbol{K}_{ms}\boldsymbol{K}_{ss}^{-1}\boldsymbol{M}_{ss}\boldsymbol{K}_{ss}^{-1}\boldsymbol{K}_{sm} \end{aligned} \tag{5}$$

$$\boldsymbol{K}_G = \boldsymbol{T}_G^{\mathrm{T}}\boldsymbol{K}\boldsymbol{T}_G = \boldsymbol{K}_{mm} - \boldsymbol{K}_{ms}\boldsymbol{K}_{ss}^{-1}\boldsymbol{K}_{sm} \tag{6}$$

The reliability of Guyan reduction in structural static analysis has been proven in engineering applications for decades. It is worth mentioning that the default method in the superelement static analysis of commercial finite element software NASTRAN is the Guyan reduction. In addition, it can also provide sufficiently accurate results in some dynamic analyses. For instance, a small avionics box that is included in an aircraft dynamic landing analysis may have modal frequencies higher than the range of interest and will respond "statically." In this case, the physical stiffness and mass of the box are important, but the dynamic mass (i.e., local frequency) is irrelevant to the solution objective. Another case when static condensation is sufficient for dynamic analysis is that the physical DOFs that are retained are sufficient to represent the dynamic response of interest. For example, a simply-supported beam with 100 grids statically reduced to 50 grids (i.e., every other grid) will be sufficient for dynamic analysis that only requires a few dozen modes.

However, since the inertia effects associated with the slave DOFs have been ignored, natural frequencies and mode shapes will be different from those of the original model [25]. The magnitude of the differences would depend on how much the inertia effects are neglected. Therefore, even if the original FE model perfectly describes the physical system (with the exact match of natural frequencies and mode shapes), the Guyan reduction introduces errors and will affect the reliability of the reduced model. Hughes's comments [26] also well revealed this fact: "A disadvantage of reduction techniques such as the Irons-Guyan procedure is that there is no guarantee that the eigenvalues and eigenvectors of the reduced problem will be good approximations of those of the original problem." In order to effectively evaluate the reliability of the reduced model and calculate the relative eigenvalue error, a simple and effective error estimation method for Guyan reduction was proposed by Kim [27, 28]. There are also other scholars who proved that the relative eigenvalue error could be avoided indirectly by using some iterative processes [22, 23, 29].

In the past two decades, scholars have carried out research in different fields using the Guyan reduction [30–34]. Li et al. [30] studied the damage detection of jacket-type offshore structures based on the Guyan reduction technology when spatially incomplete lower-order modes were given. The comparison between damage detection results based on

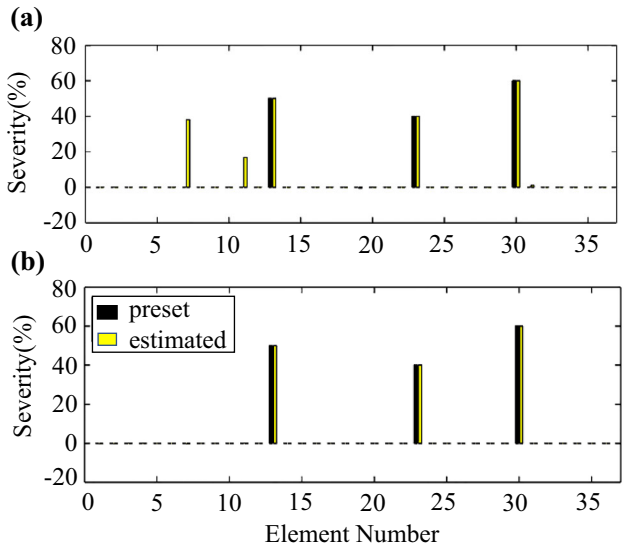

Fig. 1 Damage detection results based on the Guyan reduction approach with 36 translational DOFs: **a** without iteration; **b** with iteration [30]

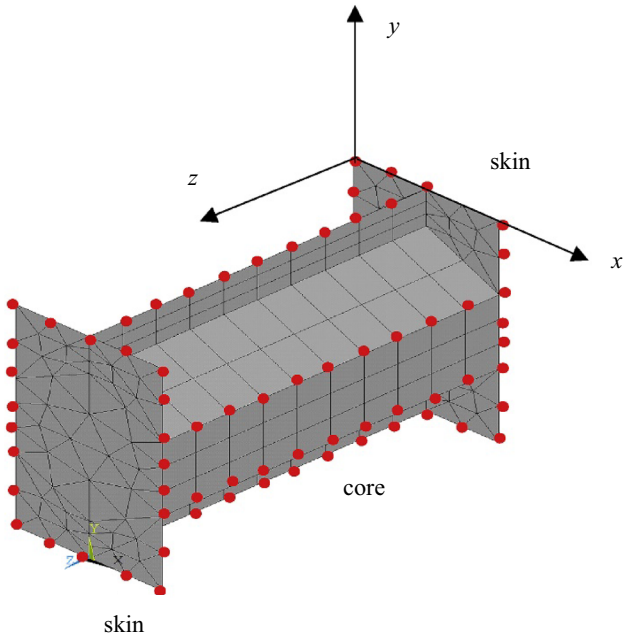

Fig. 2 FE model of a periodic cell with the master nodes marked by red dots [31]

the Guyan reduction and preset damage results is displayed in Fig. 1. The numerical results reveal that the iterative Guyan reduction can accurately locate the damage and evaluate the damage degree.

For complicated periodic structures such as corrugated core panels, laminated structures, and honeycomb-cored structures, the complicated geometry of the periodic cells leads to a huge FE model, which increases the computational consumption. When studying the sound transmission of honeycomb panels, Yang et al. [31] reduced the model size of three-dimensional periodic cells based on the Guyan reduction. Figure 2 shows the finite element model of a periodic cell, and the master nodes retained by the simplified model are marked with red dots. After the Guyan reduction, the DOFs of the reduced model are only one-third of that of the full model, while the error is less than 0.01%.

The spectral stochastic finite element method based on Polynomial Chaos (P–C) expansion is the most widely used method for the analysis of structural parameter uncertainty. The drawback of this method is the exponential growth of the computational cost with dimensionality, i.e., the number of random parameters and the order of the expansion. Therefore, how to improve computational efficiency is an urgent problem to be solved. Panayirci et al. [32] discussed the application of Guyan reduction in stochastic finite element (SFE) analysis and carried out the numerical calculation of a large building model. Table 1 shows the comparison of calculation time between standard P–C and Guyan P–C in the numerical example. It is noted that Guyan P–C can significantly improve computational efficiency.

Table 1 Comparison of computational time (in seconds). Reproduced with permission [32]

Case		Standard P–C	Guyan P–C
A	Step1	3	4
	Step2	20	35
	Step3	223	2
	Step4	392	1
	Total CPU time	638	42
B	Step1	4	7
	Step2	80	153
	Step3	893	3
	Step4	1281	2
	Total CPU time	2258	165
C	Step1	8	11
	Step2	153	305
	Step3	1738	4
	Step4	4061	3
	Total CPU time	5960	323
D	Step1	–	88
	Step2	–	1255
	Step3	–	5
	Step4	–	1709
	Total CPU time	–	3057

Model reduction is a problem that must be solved in the process of spacecraft finite element model verification. During the test for the model correlation of spacecraft, Mercer et al. [33] compared different reduction methods (including the Guyan reduction and SEREP) and proposed a sensor arrangement method in the experiment. Dynamic analysis of nonlinear structural systems is often difficult due to the large number of DOFs. With the in-depth study of reduction technology, scholars gradually found the application prospect of Guyan reduction in nonlinear systems. Zhang et al. [34] presented an investigation on the performances of nonlinear rotor-bearing-foundation systems with reduced rotor models obtained by the Guyan reduction and the mode superposition methods. The steady-state responses obtained using the reduced rotor models are compared with the responses of the original unreduced system, which shows that the Guyan reduction has good accuracy in the low-frequency range.

2.1.2 The Kidder Method

In the Guyan reduction, the transformation matrix $\boldsymbol{T}_G$ is obtained by considering only the static equation of the structure. To reduce the errors caused by ignoring the effect of inertia in the Guyan reduction, Kidder [9] proposed a new reduction method in 1973 by introducing the mass of DOFs to improve the accuracy of the Guyan reduction. In Kidder's method, the generalized eigenvalue problem of the structural system is firstly given out

$$\begin{bmatrix} \boldsymbol{K}_{mm} & \boldsymbol{K}_{ms} \\ \boldsymbol{K}_{sm} & \boldsymbol{K}_{ss} \end{bmatrix} \begin{Bmatrix} \boldsymbol{u}_m \\ \boldsymbol{u}_s \end{Bmatrix} = \lambda \begin{bmatrix} \boldsymbol{M}_{mm} & \boldsymbol{M}_{ms} \\ \boldsymbol{M}_{sm} & \boldsymbol{M}_{ss} \end{bmatrix} \begin{Bmatrix} \boldsymbol{u}_m \\ \boldsymbol{u}_s \end{Bmatrix} \tag{7}$$

where $\lambda = \omega^2$ is the eigenvalue of the structural system, and ω is the natural frequency.

Thus, from the second row, the slave DOFs $\boldsymbol{u}_s$ can be expressed as

$$\boldsymbol{u}_s = (\boldsymbol{K}_{ss} - \lambda \boldsymbol{M}_{ss})^{-1}(\lambda \boldsymbol{M}_{sm} - \boldsymbol{K}_{sm})\boldsymbol{u}_m \tag{8}$$

It is noted that Eq. (8) is the exact form of $\boldsymbol{u}_s$ considering the effect of inertia. Substituting Eq. (8) into the first row of Eq. (7), and introducing the Neumann series expansion to deal with the inverse matrix $(\boldsymbol{K}_{ss} - \lambda M_{ss})^{-1}$, the final Kidder transformation matrix $\boldsymbol{T}_K$ can be obtained as

$$\begin{aligned} \boldsymbol{u} &= \begin{Bmatrix} \boldsymbol{u}_m \\ \boldsymbol{u}_s \end{Bmatrix} \\ &= \begin{Bmatrix} \boldsymbol{I} \\ \left(\boldsymbol{K}_{ss}^{-1} + \lambda \boldsymbol{K}_{ss}^{-1} \boldsymbol{M}_{ss} \boldsymbol{K}_{ss}^{-1}\right)(\lambda \boldsymbol{M}_{sm} - \boldsymbol{K}_{sm}) \end{Bmatrix} \boldsymbol{u}_m = \boldsymbol{T}_K \boldsymbol{u}_m \end{aligned} \tag{9}$$

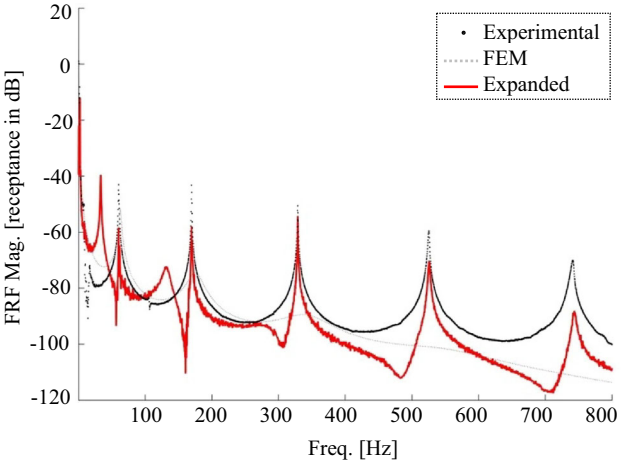

Fig. 3 Transferred FRF (H_{yb}, τ_a)—Case 1: damped FE model [36]

based on which, the reduced mass and stiffness matrices in the Kidder method are

$$\boldsymbol{M}_K = \boldsymbol{T}_K^{\mathrm{T}} \boldsymbol{M} \boldsymbol{T}_K, \quad \boldsymbol{K}_K = \boldsymbol{T}_K^{\mathrm{T}} \boldsymbol{K} \boldsymbol{T}_K \tag{10}$$

Obviously, due to the retention of the first-order inertia term, the Kidder method is more accurate than the Guyan reduction. However, the accuracy of the Kidder method depends on the selection of λ. In other words, the Kidder method is accurate at the initial frequency corresponding to the selected initial eigenvalues, and still maintains good accuracy in its nearby frequencies. However, when it is far from the initial eigenvalues, the accuracy of the natural frequency and mode shape of the reduced model will gradually decrease. The above limitation has also been mentioned in Refs. [25, 35].

Due to its limitations, the Kidder method has very limited engineering applications and theoretical research. Generally, theoretical simulation data and measurement data are not compatible in terms of the type and number of DOFs. Although the finite element model can provide complete information of DOFs, the traditional vibration test can only obtain limited information of DOFs. Therefore, it is necessary to expand the experimental data. Based on the generalized Kidder method, Maia and Silva [36] proposed a frequency response function expansion method which avoids the need for modal identification because it directly uses the measured translation frequency response. Figure 3 shows the experimental results of this method. The results show that this expansion technique has not only high accuracy but also strong robustness to noise.

2.1.3 Improved Reduction System Methods (IRS, DIRS and IIRS)

In 1989, O'Callaghan [10] improved the Guyan reduction by proposing an improved reduction system (IRS) method. The method improves the transformation from the Guyan reduction by including the inertia terms as pseudo-static forces. The transformation matrix is obtained by gradually approximating the displacement with the mode shape. By introducing binomial series expansion on frequency, Gordis [37] further generated the transformation of the standard IRS method. The theoretical derivation of the previous part of the IRS method is the same as the Kidder method. The second row of Eq. (9) can be further written as

$$\boldsymbol{u}_s = -\boldsymbol{K}_{ss}^{-1}\left[\boldsymbol{K}_{sm} + \lambda\left(\boldsymbol{M}_{ss}\boldsymbol{K}_{ss}^{-1}\boldsymbol{K}_{sm} - \boldsymbol{M}_{sm}\right) + o(\lambda^2)\right]\boldsymbol{u}_m \tag{11}$$

where λ can be approximated by the Guyan reduction as

$$\lambda \boldsymbol{M}_G \boldsymbol{u}_m = \boldsymbol{K}_G \boldsymbol{u}_m, \quad \lambda \boldsymbol{u}_m = \boldsymbol{M}_G^{-1}\boldsymbol{K}_G \boldsymbol{u}_m \tag{12}$$

Substituting Eq. (12) into Eq. (11), the transformation relationship in IRS can be obtained as

$$\boldsymbol{u}_s = \left[-\boldsymbol{K}_{ss}^{-1}\boldsymbol{K}_{sm} + \boldsymbol{K}_{ss}^{-1}\left(\boldsymbol{M}_{sm} - \boldsymbol{M}_{ss}\boldsymbol{K}_{ss}^{-1}\boldsymbol{K}_{sm}\right)\boldsymbol{M}_G^{-1}\boldsymbol{K}_G\right]\boldsymbol{u}_m \tag{13}$$

The above equation defines the transformation relationship between slave and master DOFs in the IRS method. Although it is strictly correct only when the coordinate vector is the mode shape, it may be applied as a general transformation which may be conveniently written as

$$\boldsymbol{T}_{IRS} = \boldsymbol{T}_G + \boldsymbol{S}\boldsymbol{M}\boldsymbol{T}_G\boldsymbol{M}_G^{-1}\boldsymbol{K}_G, \quad \boldsymbol{S} = \begin{bmatrix} \boldsymbol{0} & \boldsymbol{0} \\ \boldsymbol{0} & \boldsymbol{K}_{ss}^{-1} \end{bmatrix} \tag{14}$$

It is worth noting that compared with the Guyan method, the IRS reduced mass matrix is not easy to pass the cross-orthogonality check (COC), and its reduced stiffness matrix is even more rigid [37]. Therefore, in 1995, Friswell [22] further proposed the dynamic improved reduction system (DIRS) method and the iterated improved reduction system (IIRS) method. The DIRS uses the dynamic reduction instead of the Guyan reduction as the basic transformation, and the IIRS generates the correction term iteratively by introducing an iterative scheme and using the current best estimation of the reduced model. It has been proven that the natural frequencies of the reduced models of DIRS and IIRS converge to the natural frequencies of the original model [23, 38]. In addition, the calculation accuracy and convergence of the DIRS method largely depend on the selection of master DOFs. The IIRS method greatly improves the adverse effect of the selection of master DOFs.

The DIRS method can be regarded as an improvement of the dynamic reduction method [39]. The Guyan reduction is correct only statically (zero frequency). Under a determined frequency Ω, the reduced model of dynamic reduction is accurate, and the transformation can be given as

$$\boldsymbol{u} = \begin{Bmatrix} \boldsymbol{u}_m \\ \boldsymbol{u}_s \end{Bmatrix} = \begin{Bmatrix} \boldsymbol{I} \\ -\left(\boldsymbol{K}_{ss} - \Omega^2\boldsymbol{M}_{ss}\right)^{-1}\left(\boldsymbol{K}_{sm} - \Omega^2\boldsymbol{M}_{sm}\right) \end{Bmatrix} \cdot \boldsymbol{u}_m = \boldsymbol{T}_d\boldsymbol{u}_m \tag{15}$$

As for the DIRS, it is basically the same as that of the standard IRS method, except that the slave DOFs are written as a power series in $(\lambda - \Omega^2)$. The transformation can be expressed as

$$\boldsymbol{u}_s = -\boldsymbol{D}_{ss}^{-1}\left[\boldsymbol{D}_{sm} + \left(\lambda - \Omega^2\right)\left(\boldsymbol{M}_{ss}\boldsymbol{D}_{ss}^{-1}\boldsymbol{D}_{sm} - \boldsymbol{M}_{sm}\right)\right]\boldsymbol{u}_m \tag{16}$$

in which, $\boldsymbol{D}_{ss} = \boldsymbol{K}_{ss} - \Omega^2\boldsymbol{M}_{ss}$, and $\boldsymbol{D}_{sm} = \boldsymbol{K}_{sm} - \Omega^2\boldsymbol{M}_{sm}$. The reduced model based on the dynamic reduction to the first order in $(\lambda - \Omega^2)$ satisfies

$$\left(\lambda - \Omega^2\right)\boldsymbol{M}_G\boldsymbol{u}_m = \boldsymbol{D}_G\boldsymbol{u}_m, \quad \left(\lambda - \Omega^2\right)\boldsymbol{u}_m = \boldsymbol{M}_G^{-1}\boldsymbol{D}_G\boldsymbol{u}_m \tag{17}$$

where $\boldsymbol{D}_G = \boldsymbol{K}_G - \Omega^2\boldsymbol{M}_G$. Therefore, the transformation matrix of DIRS can be obtained

$$\boldsymbol{T}_{DIRS} = \boldsymbol{T}_d + \boldsymbol{S}_d\boldsymbol{M}\boldsymbol{T}_d\boldsymbol{M}_G^{-1}\boldsymbol{K}_G, \quad \boldsymbol{S}_d = \begin{bmatrix} \boldsymbol{0} & \boldsymbol{0} \\ \boldsymbol{0} & \boldsymbol{D}_{ss}^{-1} \end{bmatrix} \tag{18}$$

The transformation of Eq. (14) relies on the reduced mass and stiffness matrices obtained from the Guyan reduction. Once the transformation has been computed, an improved estimate of these reduced matrices can be updated. Therefore, the iterative calculation can be used to improve the calculation accuracy of the IRS method. The iterative calculation can be

$$\boldsymbol{T}_{IIRS,i+1} = \boldsymbol{T}_G + \boldsymbol{S}\boldsymbol{M}\boldsymbol{T}_{IIRS,i}\boldsymbol{M}_{IIRS,i}^{-1}\boldsymbol{K}_{IIRS,i} \tag{19}$$

where the subscript "i" denotes the ith iteration. It should be noted that the iterative initialization of Eq. (19) is the Guyan reduction method, and the first iteration is the IRS method, that is

$$\begin{aligned} &\boldsymbol{T}_{IIRS,0} = \boldsymbol{T}_G, \quad \boldsymbol{T}_{IIRS,1} = \boldsymbol{T}_{IRS}, \\ &\boldsymbol{M}_{IIRS,0} = \boldsymbol{M}_G, \quad \boldsymbol{K}_{IIRS,0} = \boldsymbol{K}_G \end{aligned} \tag{20}$$

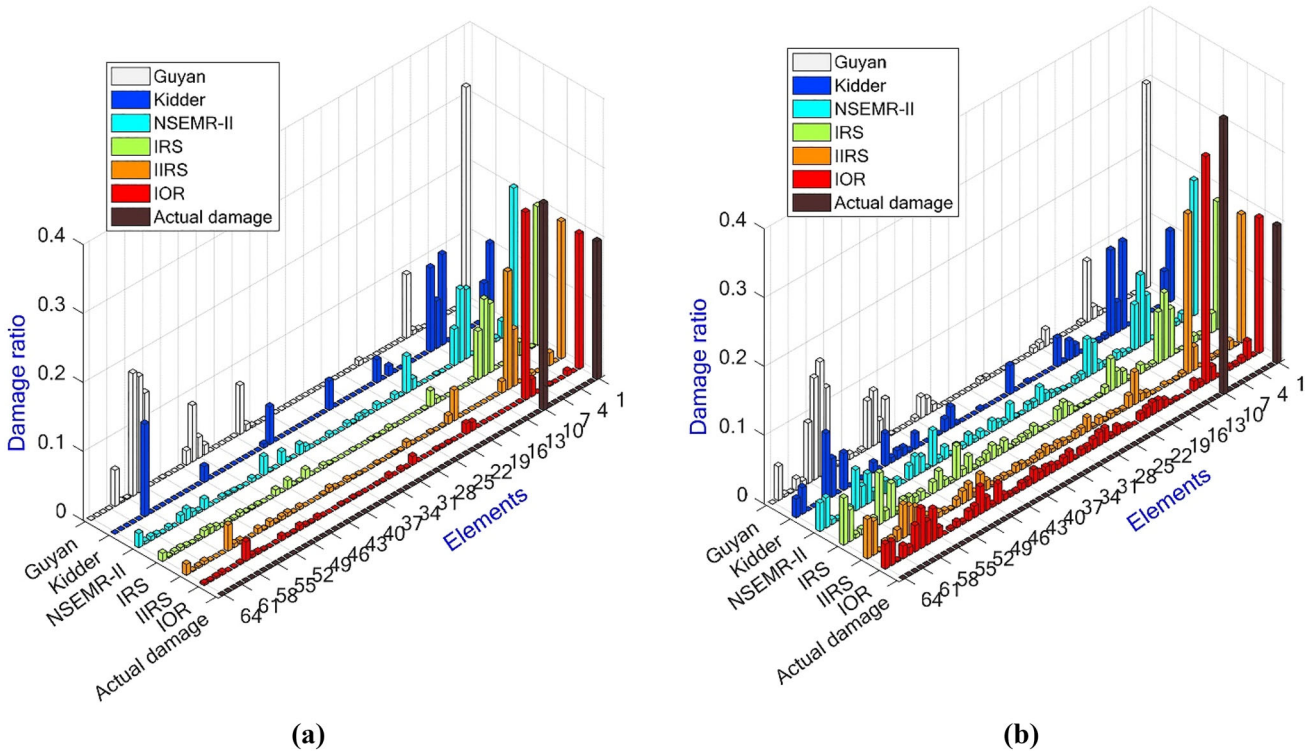

Fig. 4 Comparison of damage identification results for scenario A of the FGM plate using different dynamic condensation techniques: **a** noise-free; **b** with noise [35]

In addition, the iterated IRS technique proposed by Blair et al. [40] is different from Eq. (19) as

$$\boldsymbol{T}_{IIRS,i+1} = \boldsymbol{T}_G + \boldsymbol{SMT}_G \boldsymbol{M}_{IIRS,i}^{-1} \boldsymbol{K}_{IIRS,i} \tag{21}$$

where the Guyan transformation is retained in the second term of the right-hand side. The algorithm defined by Eq. (21) converges to yield reduced mass and stiffness matrices that do not reproduce the eigenvalues of the full system. In addition, the DIRS method can be easily extended to the iterative form similar to Eq. (19).

The IRS method has been widely used in damage identification, structural nonlinearity, topology optimization, and many other fields because of its high accuracy [41–47]. Dinh-Cong et al. [35] studied the damage identification of functionally graded materials (FGM) by using six reduction techniques, i.e., the Guyan reduction method, the Kidder method, the Neumann series expansion-based second-order model reduction (NSEMR-II) method, the IRS method, the IIRS method, and the iterative order reduction (IOR) method. The FGM damage identification results of different reduction techniques are shown in Fig. 4. The results show that the IIRS method can effectively solve the problem of structural damage identification, while the Kidder method has a poor damage identification effect.

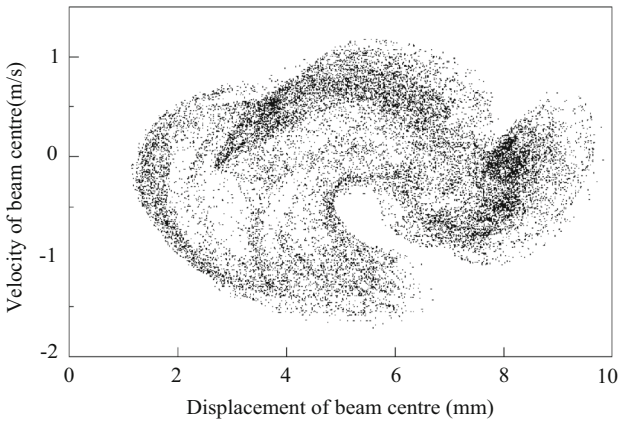

Fig. 5 Poincaré map for the pinned beam with 16 DOFs [41]

Friswell et al. [41] studied the finite element model reduction of structures with local nonlinearities using the IRS method, which is the first application of the IRS method in the field of structural nonlinearity. Figure 5 shows the Poincaré map of the reduced nonlinear model, which is very similar to the full model. Based on the section damage modeling of the IIRS method, an effective method for cross-sectional damage localization and quantification in beams was proposed by Hosseinzadeh et al. [42] This method can be applied by

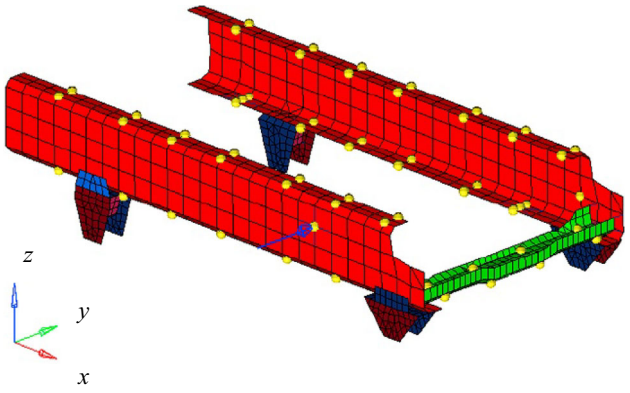

Fig. 6 FEM model of the front part of a vehicle frame [43]

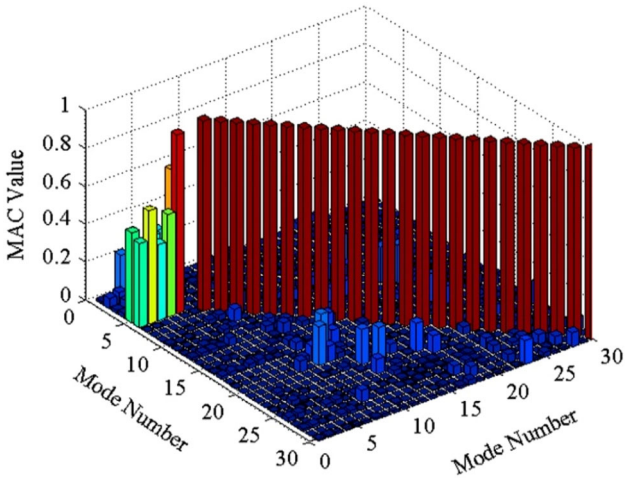

Fig. 7 3D presentation of MAC values [43]

utilizing incomplete modal data or installing a limited number of sensors for damage identification. The results show that the method not only can accurately locate all simulated damage but also has good robustness to noise.

In order to improve the calculation efficiency of large-scale finite element models, Xie et al. [43] studied the model reduction of vehicles by using the IIRS method. Only 66 nodes are selected as the master nodes which are highlighted in Fig. 6. Only the translational DOFs of the master nodes are retained in the reduction process. Figure 7 shows a three-dimensional representation of modal assurance criterion (MAC) values between the reduced and the original full models. It is found that the IIRS method tends to generate better reduction approximation.

Based on the stochastic finite element method (SFEM) and the IIRS method, Ni et al. [44] performed the stochastic dynamic response analysis of marine risers with uncertain mass density and elastic modulus. Figure 8 shows the SFEM results with and without model reduction. These results are

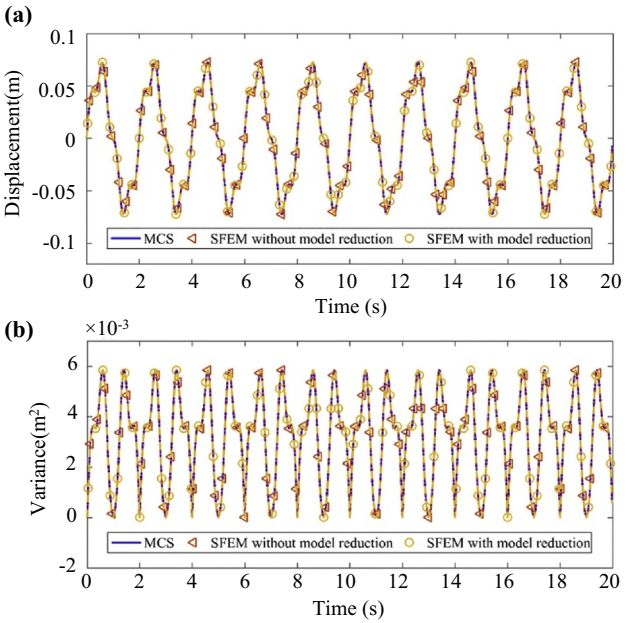

Fig. 8 Response statistics of the displacement at the critical point along the y-direction from the SFEM with/without mode reduction: **a** mean value; **b** variance [44]

consistent with the results obtained by Monte Carlo simulation (MCS), while the calculation time required for the full model and reduced model is 5974 s and 1944s, respectively. These results show that the IIRS method has no significant impact on the accuracy of random response analysis but significantly shortens the calculation time.

2.1.4 System Equivalent Reduction Expansion Process (SEREP)

In 1989, O'Callahan et al. [11] proposed the system equivalent reduction expansion process (SEREP). Different from the above-mentioned three methods, SEREP is developed based on modal coordinates. O'Callahan and Li [48] further improved the SEREP technique by introducing the concept of generalized inverse. The SEREP is a reduction transformation based on a subset of the modes of the full model, and the reduced model exactly describes the selected modes at the chosen master DOFs [49]. It allows matching the DOFs between numerical mode shapes and experimental mode shapes without losing dynamic characteristics. The essence of SEREP method is to establish a transformation matrix obtained by modal reduction. The generalized eigenvalue problem of structural systems can be written as

$$\begin{bmatrix} \boldsymbol{K}_{mm} & \boldsymbol{K}_{ms} \\ \boldsymbol{K}_{sm} & \boldsymbol{K}_{ss} \end{bmatrix} \begin{Bmatrix} \boldsymbol{\Phi}_m \\ \boldsymbol{\Phi}_s \end{Bmatrix} \boldsymbol{q} = \lambda \begin{bmatrix} \boldsymbol{M}_{mm} & \boldsymbol{M}_{ms} \\ \boldsymbol{M}_{sm} & \boldsymbol{M}_{ss} \end{bmatrix} \begin{Bmatrix} \boldsymbol{\Phi}_m \\ \boldsymbol{\Phi}_s \end{Bmatrix} \boldsymbol{q} \quad (22)$$

in which, $\boldsymbol{\Phi}_m$ and $\boldsymbol{\Phi}_s$ are the modal matrices of the master and slave DOFs, respectively, and $\boldsymbol{q}$ is the generalized coordinate. The relationship between coordinates in physical space and modal space is

$$\begin{Bmatrix} \boldsymbol{u}_m \\ \boldsymbol{u}_s \end{Bmatrix} = \begin{Bmatrix} \boldsymbol{\Phi}_m \\ \boldsymbol{\Phi}_s \end{Bmatrix} \boldsymbol{q} \tag{23}$$

from which, by eliminating the rows corresponding to the slave DOFs, one can have

$$\boldsymbol{q} = \boldsymbol{\Phi}_m^{+} \boldsymbol{u}_m \tag{24}$$

where the superscript "+" represents the generalized inverse of matrix. As a result, the transformation matrix $\boldsymbol{T}_S$ of SEREP is

$$\boldsymbol{T}_S = \begin{Bmatrix} \boldsymbol{\Phi}_m \\ \boldsymbol{\Phi}_s \end{Bmatrix} \boldsymbol{\Phi}_m^{+} \tag{25}$$

In general, the modal matrices have orthogonality, so the reduced mass and stiffness matrices for SEREP can be obtained as

$$\begin{aligned} \boldsymbol{M}_S &= \boldsymbol{T}_S^{\mathrm{T}} \boldsymbol{M} \boldsymbol{T}_S = \left(\boldsymbol{\Phi}_m^{+}\right)^{\mathrm{T}} \boldsymbol{\Phi}_m^{+}, \\ \boldsymbol{K}_S &= \boldsymbol{T}_S^{\mathrm{T}} \boldsymbol{K} \boldsymbol{T}_S = \left(\boldsymbol{\Phi}_m^{+}\right)^{\mathrm{T}} \mathrm{diag}(\lambda) \boldsymbol{\Phi}_m^{+} \end{aligned} \tag{26}$$

It should be emphasized that the SEREP method can handle free and clamped boundary conditions for both finite element numerical models and experimental data [50]. In addition, an important feature of SEREP is that it is not necessary to model the structure by FEM in advance. Based on the modal shape of theoretical analysis or experimental measurement, the reduced dynamic system can be obtained arbitrarily, as shown in Eq. (26). On the contrary, by using the SEREP transformation matrix of the coupled FE model, the unmeasured DOFs can be predicted from the measured experimental mode, which is known as the virtual sensing [11].

The SEREP method uses mode shapes instead of static equations to generate a reduced matrix. Therefore, it is widely used in damage detection and fault identification, active control, model reduction of complex systems, cross-orthogonality check between analytical and experimental modal vectors, linear and nonlinear forced response studies, and analytical model improvement [51–60]. Ghannadi and Kourehli [51] proposed a model-based structural element damage detection and severity identification method, using the extended mode shape data based on the SEREP method to train the artificial neural network to solve the problem of limited number of sensors. Figure 9 shows the comparison between the predicted results and the actual results in three different cases of 30-element plane truss. It can be observed that the method can predict the severity and location of damage accurately.

Fault detection of rotating machinery is a classical subject of rotor dynamics. Sanches and Pederiva [52] proposed a time-domain identification method based on correlation analysis and the SEREP model reduction to estimate the concurrent faults synchronized with the speed of rotor. Numerical examples and experimental data were used to verify the feasibility of the method.

The DOFs in FE models of rotor shaft structures are usually huge, so it is often very difficult to actively control due to the time delay caused by high calculation costs. Das and Dutt [53, 54] reduced the rotor shaft system model by the SEREP method and then successfully used the reduced model to control the rotor shaft actively. The results show that the reduction model can greatly reduce the computational cost of active control.

There are many asymmetric factors in the propeller shaft system, such as the gyro effect, internal damping, and journal support. A large number of states of these high-order models and the existence of asymmetry make the post-processing of the system complex. Ganguly and Roy [55] solved these limitations by using the improved SEREP method to reduce the hollow propeller shafting model. Figure 10 compares the steady-state time response for the full and reduced models in the unstable zone considering the spin speed of rotor as 2000 rpm. The comparative results show a perfect reduction of the full model system.

Engineering structures are prone to fatigue failure under the action of working impulse. Obtaining the overall stress information is the key to estimating the residual fatigue life of structures. Unfortunately, it is very difficult to install sensors at the key locations of fatigue, and sensors are usually damaged by the working environment. For the fatigue analysis of engineering structures, virtual sensing is usually used. In order to predict the global vibration response of the interstage piping system of the compound compressor, Mendonsa et al. [56] proposed an extended virtual sensing methodology based on the SEREP method. The specific steps of the virtual sensing technology are introduced in Fig. 11. Similar virtual sensing methods were also applied to predict the residual fatigue life of offshore structures [57]. Based on the SEREP method, Thibault et al. [58] proposed a computationally efficient technique-equivalent reduced model technique (ERMT), which utilizes reduced linear component models assembled with discrete nonlinear connection elements to perform nonlinear forced response analysis.

In addition, the SEREP method is also applied to the model reduction of the fluid–structure coupling system. Lal et al. [59] proposed a reduced-order model based on the parallel method of SEREP and polynomial chaos expansion to analyze the fluid–structure coupling system with

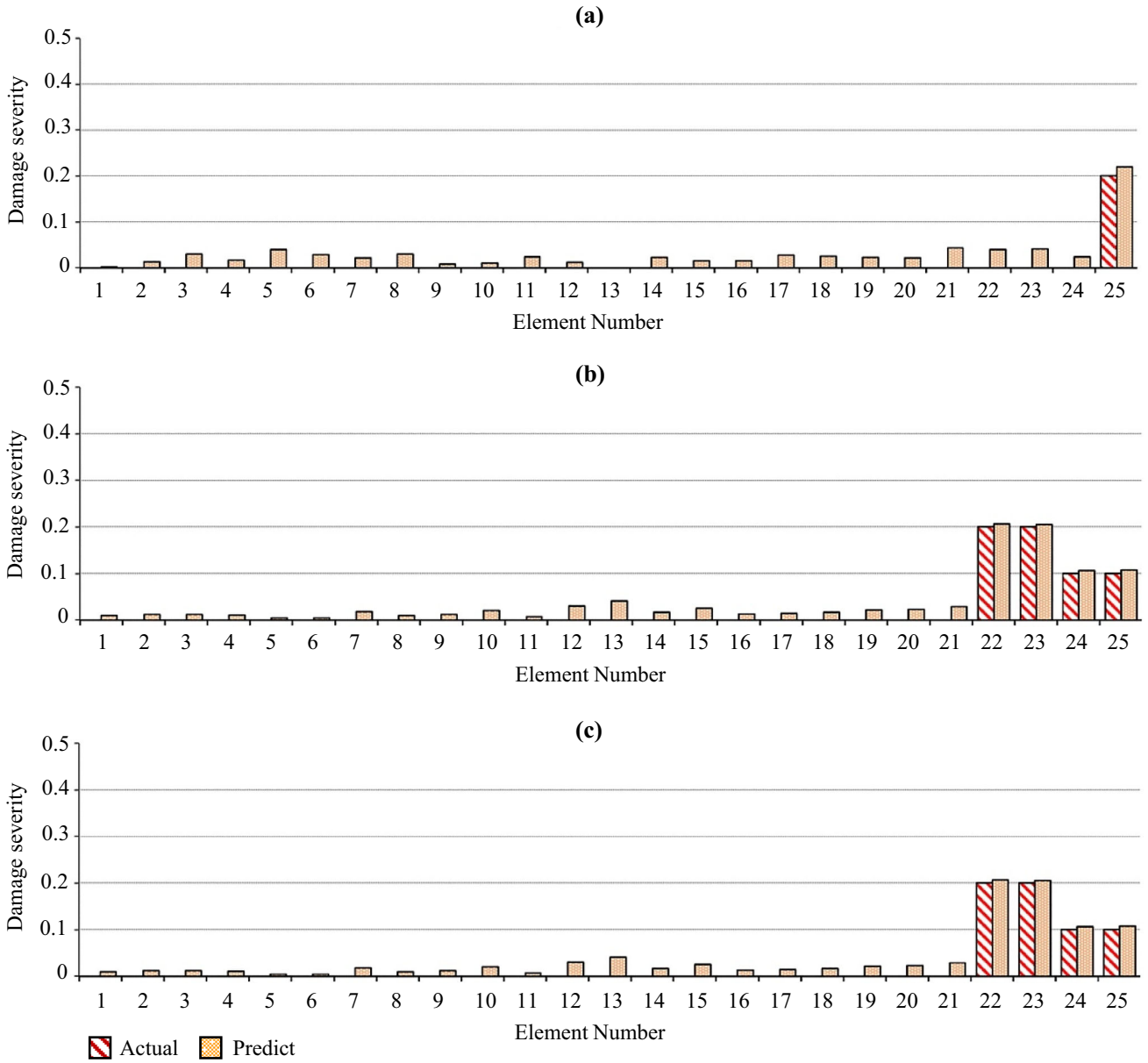

Fig. 9 Results of damage prediction for space truss with 25 elements: **a** damage element is 25; **b** damage elements are 22, 23, 24, and 25; **c** damage elements are 1, 4, 6, 7, 8, and 9 [51]

random parameter uncertainty. Numerical results reveal that the proposed method results in a significant reduction in computational cost for dynamic analysis without compromising on accuracy. Sarkar and Venkatraman [60] applied the SEREP method to the model order reduction of linear unsteady aerodynamic problems. The numerical results show that this method is more effective than the proper orthogonal decomposition (POD) method in determining the response of the unsteady aerodynamic model of the vibrating airfoil cascade.

2.2 Component Mode Synthesis (CMS) Method

The component mode synthesis (CMS) method, also known as the dynamic substructure method, relies on a combination of physical and mode base vectors to form the reduced subspace [61–65]. The basic idea is to "divide and conquer", that is, to divide the original structure into some substructures according to certain rules, and perform relevant operations (design, modeling, model reduction, etc.) on the substructures. In the process of the substructure from segmentation to assembly, the reduction of DOFs must run through all the time. At the same time, the accuracy of the analysis must be

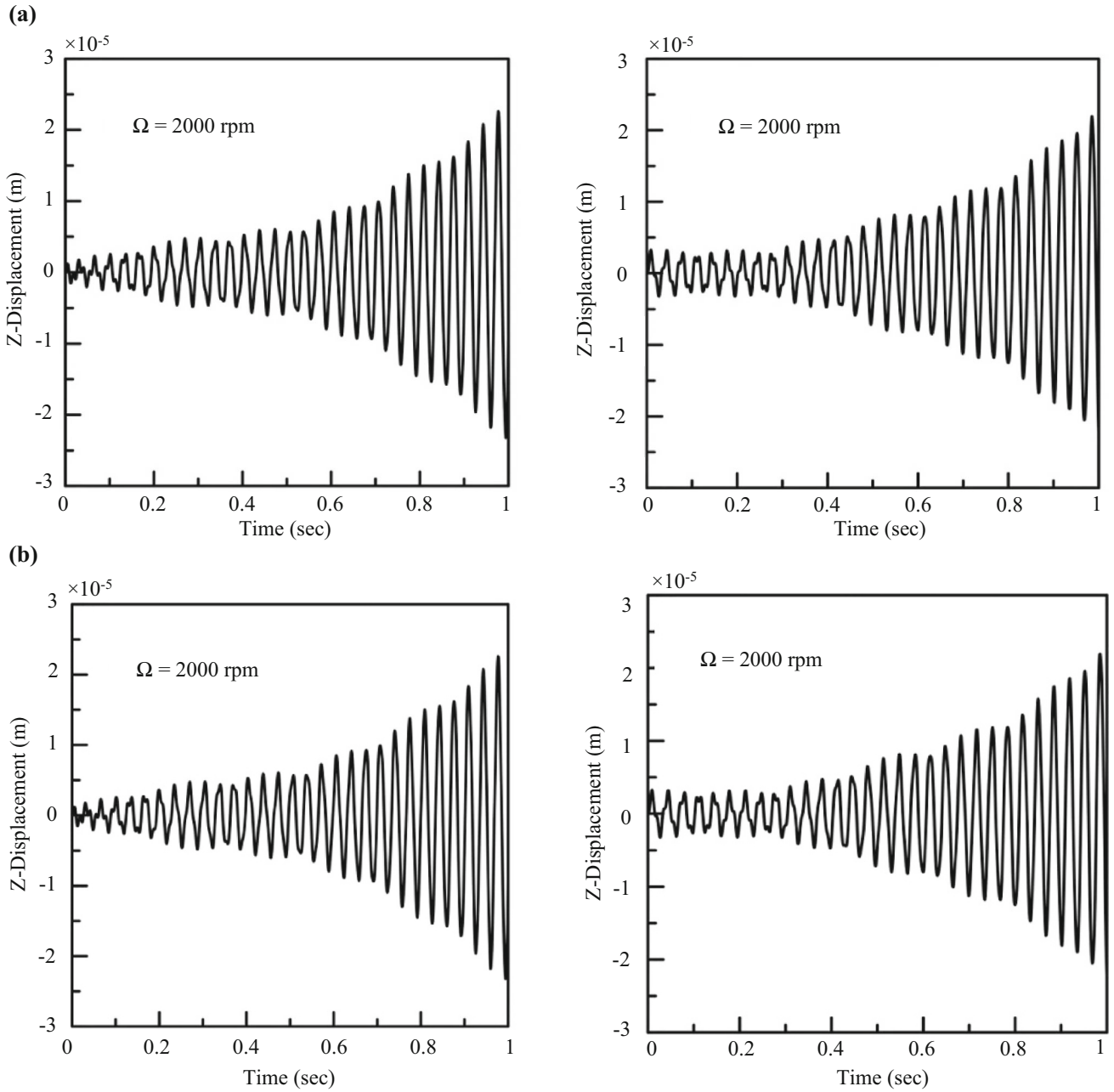

Fig. 10 Time-response plot for unstable zone at Ω = 2000 rpm: **a** full model; **b** reduced model [55]

guaranteed and converge with the increase in the number of DOFs involved. The ideal situation is to obtain high accuracy with the least participation DOFs The implementation process is relatively simple, which is the original intention of the CMS method. With the deepening of research, the CMS method mainly develops into three types according to the constraints on the interface of substructures: the fixed interface component mode synthesis method [12, 66], the free interface component mode synthesis method [67–70], and the mixed interface component mode synthesis method [14].

2.2.1 Fixed Interface Component Mode Synthesis Method (the Craig–Bampton Method)

The fixed interface component mode synthesis method was firstly proposed by Hurty [66] in 1965. The fixed-interface principal mode, constraint mode, and rigid body mode are used to form a complete mode set of the substructure, and the displacement coordination among the substructures is realized through the interface coordinates. Craig and Bampton [12] improved the Hurty method and formed the most widely used Craig-Bampton method at present. They pointed out that

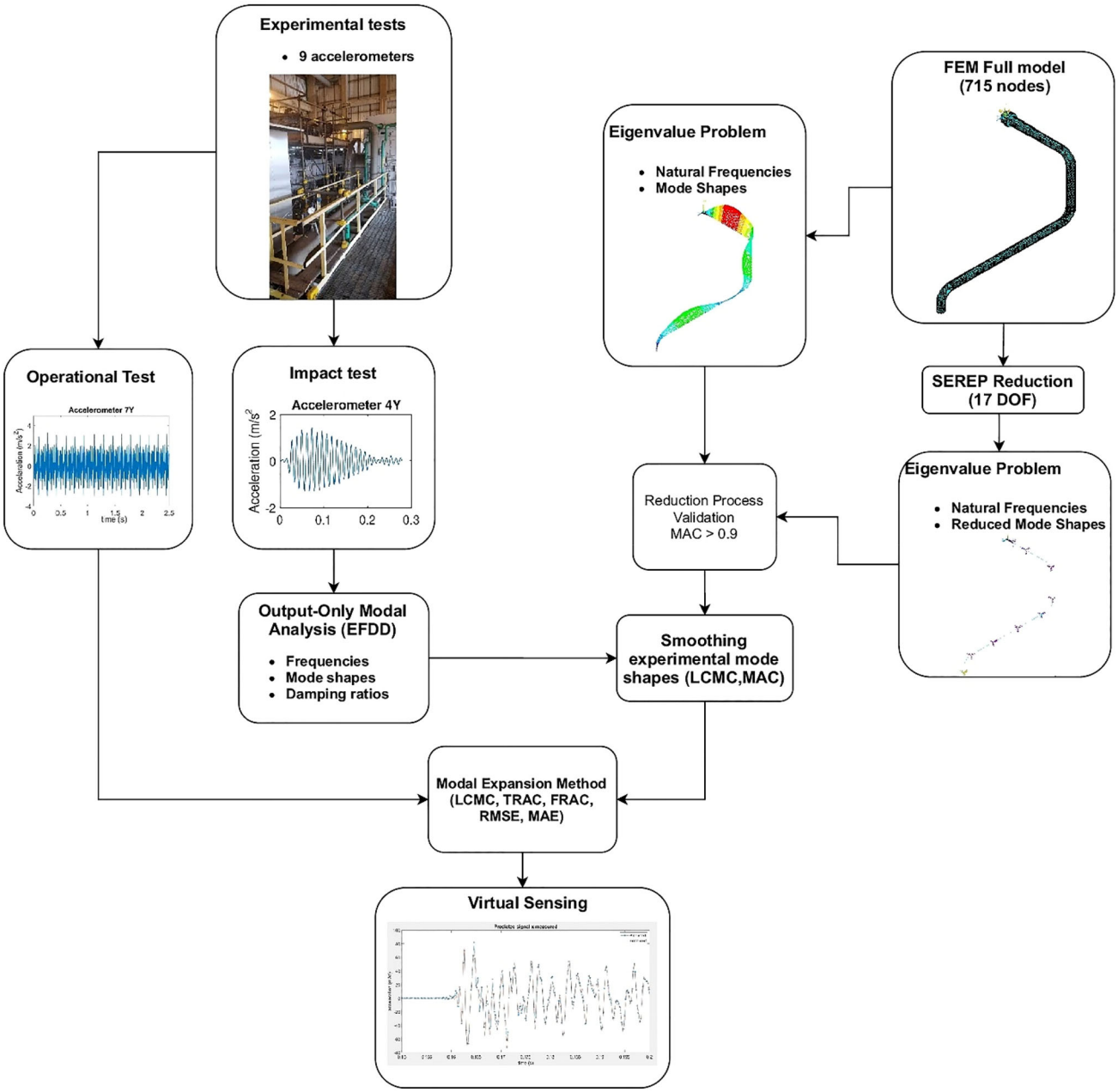

Fig. 11 Flowchart of the methodology proposed for dynamic response prediction in the compressor's interstage pipe [56]

as long as the number of constraint modes exceeds the rigid body DOFs of the substructure, the rigid body modes of the substructure will be included in the constraint modes. Therefore, it is not necessary to introduce the rigid body modes of the substructure into the hypothetical mode set alone.

The basic principle of the fixed interface component mode synthesis method is that all the interfaces between substructures are constrained, and then the modes of each constrained substructure can be obtained. According to the connection conditions of the interface, the non-independent modal coordinates are eliminated, and the comprehensive equation of the overall structure is obtained. Firstly, a diagram shown in Fig. 12 is used to explain the concepts of substructure and interface DOFs. As shown in the figure, the overall structure $\boldsymbol{S}$ is divided into substructure $\boldsymbol{S}_1$ and substructure $\boldsymbol{S}_2$, connected by the interface boundary (the red line in Fig. 12). The nodes on the interface boundary are called interface nodes, and the DOFs of interface nodes are called interface DOFs. Nodes outside the interface boundary are called interior nodes, and their DOFs are called interior DOFs.

For each substructure, the equation of motion is written in terms of the interface and interior DOFs as

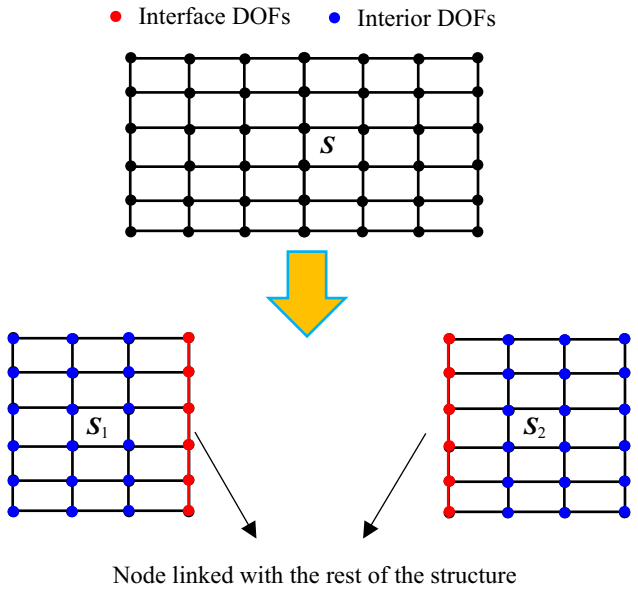

Fig. 12 Schematic diagram of the definition of substructure and interface DOFs

$$\begin{bmatrix} \boldsymbol{M}_{II} & \boldsymbol{M}_{IB} \\ \boldsymbol{M}_{BI} & \boldsymbol{M}_{BB} \end{bmatrix} \begin{Bmatrix} \ddot{\boldsymbol{u}}_I \\ \ddot{\boldsymbol{u}}_B \end{Bmatrix} + \begin{bmatrix} \boldsymbol{K}_{II} & \boldsymbol{K}_{IB} \\ \boldsymbol{K}_{BI} & \boldsymbol{K}_{BB} \end{bmatrix} \begin{Bmatrix} \boldsymbol{u}_I \\ \boldsymbol{u}_B \end{Bmatrix} = \begin{Bmatrix} \boldsymbol{F}_I \\ \boldsymbol{F}_B + \boldsymbol{R}_B \end{Bmatrix} \tag{27}$$

where the subscripts "I" and "B" denote interior and interface DOFs of the substructure, respectively; and $\boldsymbol{R}_B$ is the connection load between substructures. When analyzing a substructure, it is equivalent to the external load of the substructure.

Different from the dynamic condensation methods, the DOFs of interior nodes are composed of two parts as

$$\boldsymbol{u}_I = \boldsymbol{u}^{IB} + \boldsymbol{u}^{II} \tag{28}$$

where $\boldsymbol{u}^{IB}$ is produced by the interface DOFs, which can be approximated by the Guyan reduction as

$$\boldsymbol{u}^{IB} = -\boldsymbol{K}_{II}^{-1}\boldsymbol{K}_{IB}\boldsymbol{u}_B \tag{29}$$

As for $\boldsymbol{u}^{II}$, actually, it can be obtained using the mode superposition principle under completely constraining the interface DOFs of the substructure, i.e., $\boldsymbol{u}_B = 0$. Therefore, the equation of motion for the constrained substructure can be obtained as

$$\boldsymbol{M}_{II}\ddot{\boldsymbol{u}}^{II} + \boldsymbol{K}_{II}\boldsymbol{u}^{II} = \boldsymbol{F}_I \tag{30}$$

Solving the eigenvalue problem of Eq. (30), the displacement in physical space can be transformed to the normalized mode space as

$$\boldsymbol{u}^{II} = \boldsymbol{\Phi}_{II}\tilde{\boldsymbol{v}}_N = \left\{\boldsymbol{\Phi}_{II}^L, \boldsymbol{\Phi}_{II}^H\right\}\begin{Bmatrix} \boldsymbol{x}_N \\ \boldsymbol{x}_H \end{Bmatrix} \approx \boldsymbol{\Phi}_{II}^L\boldsymbol{x}_N \tag{31}$$

where $\tilde{\boldsymbol{v}}_N$ is the coordinate vector in normalized mode space. It can be seen from the above equation that the normalized modes are divided into the lower-order (with superscript "L") and higher-order (with superscript "H") parts; and in dynamic analysis, the high-order parts are usually truncated. As a result, the displacement vector of the substructure can be expressed as

$$\begin{aligned} \boldsymbol{u} &= \begin{Bmatrix} \boldsymbol{u}_I \\ \boldsymbol{u}_B \end{Bmatrix} = \begin{bmatrix} \boldsymbol{\Phi}_{II}^L & -\boldsymbol{K}_{II}^{-1}\boldsymbol{K}_{IB} \\ \boldsymbol{0} & \boldsymbol{I} \end{bmatrix} \begin{Bmatrix} \boldsymbol{x}_N \\ \boldsymbol{u}_B \end{Bmatrix} \\ &= \begin{bmatrix} \boldsymbol{\Phi}_{II}^L & \boldsymbol{\Phi}_{IB} \\ \boldsymbol{0} & \boldsymbol{I} \end{bmatrix} \begin{Bmatrix} \boldsymbol{x}_N \\ \boldsymbol{u}_B \end{Bmatrix} = \boldsymbol{\Phi}_c \begin{Bmatrix} \boldsymbol{x}_N \\ \boldsymbol{u}_B \end{Bmatrix} = \boldsymbol{\Phi}_c \begin{Bmatrix} \boldsymbol{P}_I \\ \boldsymbol{P}_B \end{Bmatrix} \end{aligned} \tag{32}$$

where $\boldsymbol{\Phi}_c$ is the first transformation matrix in the fixed interface component mode synthesis, based on which, the mass, stiffness and external load matrices become

$$\overline{\boldsymbol{M}} = \boldsymbol{\Phi}_c^{\mathrm{T}}\boldsymbol{M}\boldsymbol{\Phi}_c = \begin{bmatrix} \boldsymbol{I} & \overline{\boldsymbol{M}}_{IB} \\ \overline{\boldsymbol{M}}_{BI} & \overline{\boldsymbol{M}}_{BB} \end{bmatrix}, \overline{\boldsymbol{K}} = \boldsymbol{\Phi}_c^{\mathrm{T}}\boldsymbol{K}\boldsymbol{\Phi}_c = \begin{bmatrix} \boldsymbol{\Lambda}_{II} & \boldsymbol{0} \\ \boldsymbol{0} & \overline{\boldsymbol{K}}_{BB} \end{bmatrix}$$

$$\overline{\boldsymbol{F}} = \boldsymbol{\Phi}_c^{\mathrm{T}}\begin{Bmatrix} \boldsymbol{F}_I \\ \boldsymbol{F}_B + \boldsymbol{R}_B \end{Bmatrix} = \begin{Bmatrix} \left(\boldsymbol{\varphi}_{II}^L\right)^{\mathrm{T}}\boldsymbol{F}_I \\ \boldsymbol{\varphi}_{IB}^{\mathrm{T}}\boldsymbol{F}_I + \boldsymbol{F}_B + \boldsymbol{R}_B \end{Bmatrix} \tag{33}$$

Finally, the equation of motion for substructures after the first transformation is

$$\overline{\boldsymbol{M}}\ddot{\boldsymbol{P}} + \overline{\boldsymbol{K}}\boldsymbol{P} = \overline{\boldsymbol{F}} \tag{34}$$

where $\boldsymbol{P} = \{\boldsymbol{P}_I, \boldsymbol{P}_B\}^{\mathrm{T}}$ is the coordinate vector in the modal space. Actually, $\boldsymbol{P}$ is a generalized coordinate vector, because $\boldsymbol{P}_I = \boldsymbol{x}_N$ is the normalized mode coordinate, while $\boldsymbol{P}_B = \boldsymbol{u}_B$ is just the physical coordinate.

The equation of motion for the whole structure can be obtained by combining the equations of motion for all substructures as

$$\begin{bmatrix} \overline{\boldsymbol{M}}_1 & \boldsymbol{0} \\ \boldsymbol{0} & \overline{\boldsymbol{M}}_2 \end{bmatrix} \begin{Bmatrix} \ddot{\boldsymbol{P}}_1 \\ \ddot{\boldsymbol{P}}_2 \end{Bmatrix} + \begin{bmatrix} \overline{\boldsymbol{K}}_1 & \boldsymbol{0} \\ \boldsymbol{0} & \overline{\boldsymbol{K}}_2 \end{bmatrix} \begin{Bmatrix} \boldsymbol{P}_1 \\ \boldsymbol{P}_2 \end{Bmatrix} = \begin{Bmatrix} \overline{\boldsymbol{F}}_1 \\ \overline{\boldsymbol{F}}_2 \end{Bmatrix} \tag{35}$$

where the subscripts "1" and "2" represent substructures 1 and 2, respectively. The overall coordinate vector is

$$\begin{Bmatrix} \boldsymbol{P}_1 \\ \boldsymbol{P}_2 \end{Bmatrix} = \begin{Bmatrix} \boldsymbol{P}_{I,1} & \boldsymbol{P}_{B,1} & \boldsymbol{P}_{I,2} & \boldsymbol{P}_{B,2} \end{Bmatrix}^{\mathrm{T}} \tag{36}$$

where according to the continuity conditions between substructures, one can have $\boldsymbol{P}_{B,1} = \boldsymbol{P}_{B,2}$. As a result, the coordinate vector of the whole structure can be rewritten as

$$\begin{Bmatrix} \boldsymbol{P}_{I,1} \\ \boldsymbol{P}_{B,1} \\ \boldsymbol{P}_{I,2} \\ \boldsymbol{P}_{B,2} \end{Bmatrix} = \begin{bmatrix} \boldsymbol{I} & \boldsymbol{0} & \boldsymbol{0} \\ \boldsymbol{0} & \boldsymbol{0} & \boldsymbol{I} \\ \boldsymbol{0} & \boldsymbol{I} & \boldsymbol{0} \\ \boldsymbol{0} & \boldsymbol{0} & \boldsymbol{I} \end{bmatrix} \begin{Bmatrix} \boldsymbol{P}_{I,1} \\ \boldsymbol{P}_{I,2} \\ \boldsymbol{P}_{B} \end{Bmatrix} = \boldsymbol{T}_c \boldsymbol{P} \tag{37}$$

where $\boldsymbol{T}_c$ is the second transformation matrix, based on which, the final reduced FE model is

$$\overline{\overline{\boldsymbol{M}}}\ddot{\boldsymbol{P}} + \overline{\overline{\boldsymbol{K}}}\boldsymbol{P} = \overline{\overline{\boldsymbol{F}}} \tag{38}$$

where.

$$\overline{\overline{\boldsymbol{M}}} = \boldsymbol{T}_c^{\mathrm{T}} \begin{bmatrix} \overline{\boldsymbol{M}}_1 & \boldsymbol{0} \\ \boldsymbol{0} & \overline{\boldsymbol{M}}_2 \end{bmatrix} \boldsymbol{T}_c, \quad \overline{\overline{\boldsymbol{K}}} = \boldsymbol{T}_c^{\mathrm{T}} \begin{bmatrix} \overline{\boldsymbol{K}}_1 & \boldsymbol{0} \\ \boldsymbol{0} & \overline{\boldsymbol{K}}_2 \end{bmatrix} \boldsymbol{T}_c,$$

$$\overline{\overline{\boldsymbol{F}}} = \boldsymbol{T}_c^{\mathrm{T}} \begin{Bmatrix} \overline{\boldsymbol{F}}_1 \\ \overline{\boldsymbol{F}}_2 \end{Bmatrix} = \begin{Bmatrix} \left(\boldsymbol{\varphi}_{II,1}^{L}\right)^{\mathrm{T}} \boldsymbol{F}_{I,1} \\ \left(\boldsymbol{\varphi}_{II,2}^{L}\right)^{\mathrm{T}} \boldsymbol{F}_{I,2} \\ \boldsymbol{\varphi}_{IB,1}^{\mathrm{T}} \boldsymbol{F}_{I,1} + \boldsymbol{F}_{B,1} + \boldsymbol{\varphi}_{IB,2}^{\mathrm{T}} \boldsymbol{F}_{I,2} \\ + \boldsymbol{F}_{B,2} + \boldsymbol{R}_{B,1} + \boldsymbol{R}_{B,2} \end{Bmatrix} \tag{39}$$

in which, $\boldsymbol{R}_{B,1} + \boldsymbol{R}_{B,2} = 0$, because they are internal forces for the whole structure.

Another issue worth discussing is data recovery. Based on the above reduced equation of motion, the dynamic analysis of the structure system can be conducted. After that, the mode shape of the structure in the modal space should be converted to the physical space by

$$\begin{Bmatrix} \boldsymbol{u}_{I,1} \\ \boldsymbol{u}_{B,1} \\ \boldsymbol{u}_{I,2} \\ \boldsymbol{u}_{B,2} \end{Bmatrix} = \begin{bmatrix} \boldsymbol{\Phi}_{c,1} & \boldsymbol{0} \\ \boldsymbol{0} & \boldsymbol{\Phi}_{c,2} \end{bmatrix} \boldsymbol{T}_c \boldsymbol{P} \tag{40}$$

This method of directly using the modal coordinate transformation matrix is called the mode displacement (MD) method [71]. This method ignores the influence of high-order modes. If there are many higher-order components in the practical vibration, the calculation accuracy will be reduced. Other data recovery technologies will be discussed in detail in Sect. 3.3.

In recent years, scholars have also done a lot of research on the engineering application of the fixed interface component mode synthesis method [72–80]. Vizzini et al. [72] used the C-B method to reduce the order of the Volvo V40 body-in-white (BIW) structure model and carried out the vibration analysis. The results show that the simulation time can be reduced by 90% by using the CMS method instead of the complete finite element model. In order to predict the damage of composite laminates, Mahmoudi et al. [73] proposed a damage location and quantification method based on the artificial neural network (ANN) and the Craig-Bampton method. This method only needs to monitor the stress state of the composite structure. Figure 13 compares the results provided by the full damage model with those given by the ANNs. The ANNs show good agreement with the results obtained via the full model.

Generally, the control of a large-scale adaptive civil engineering structure is often challenging due to signal transmission delay. Wagner et al. [74] developed a decentralized control scheme to solve this problem. The scheme subdivides the large structure into local substructures using the Craig-Bampton method and controls the substructures separately. Taking the control of an adaptive high-rise structure as an example, the effectiveness of the scheme was illustrated. Reducing the complex model of multiple physical fields is an important step in the design and optimization of high-tech systems. Nachtergaele et al. [75] extended the classical Craig-Bampton method to the thermo-mechanical system to reduce the model of the thermo-mechanical system. Based on a simple thermal actuator model, the effectiveness of this method was verified. Figure 14 shows the accurate calculation results of the thermal-driven approach. Junge et al. [76] applied the Craig-Bampton method to simulate the low-frequency vibration acoustic behavior of fluid–structure coupled systems. It is shown that the method is capable of significantly accelerating the solution process, while introducing only a small additional error.

For nonlinear high-rise buildings, Fang et al. [77] proposed an adaptive modified numerical method based on the Craig-Bampton method to simplify the model and solve the structural dynamic response efficiently. This method can be applied to the judgment of nonlinear structural members of high-rise buildings under strong earthquake excitation. Figure 15 shows the displacement of structural roof under 620-gal ground acceleration. The results obtained by the adaptive modified Craig-Bampton method and the time step integration method are in good agreement. In addition, the Craig-Bampton method is widely used in the field of aerospace. Thomas et al. [78] developed a hybrid stick model based on the Guyan method and the Craig-Bampton method, and took the Bombardier aircraft platform as an example to carry out a dynamic aeroelastic analysis. Based on an enhanced Craig-Bampton (ECB) method, Lim et al. [79] conducted a coupled dynamic load analysis (CDLA) of the satellite to predict its maximum response (acceleration, displacement, and stress). By combining the Craig-Bampton method with the Monte Carlo simulation, Remedia et al. [80] proposed an analytical method to evaluate the dynamic

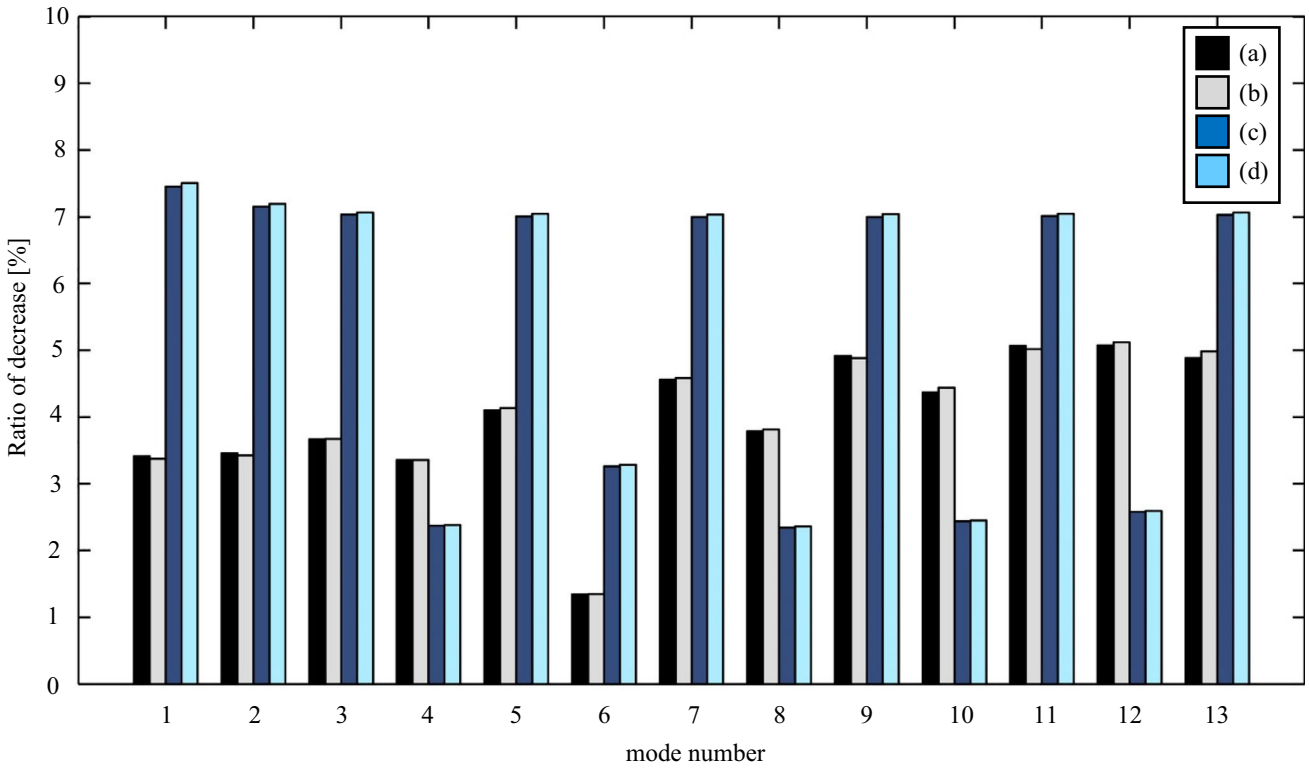

Fig. 13 Damage severity performance: **a** and **b** are the decrease ratios obtained via the full damage model and the ANN metamodel of the (45°/0°/−45°) laminated beam; **c** and **d** are the same corresponding ratios of the (90°/0°/−90°) laminated beam [73]

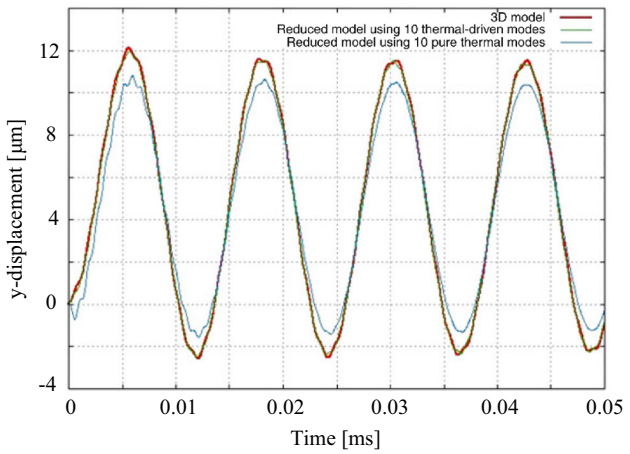

Fig. 14 Transient analysis of 200-μm model with low heat capacitance [75]

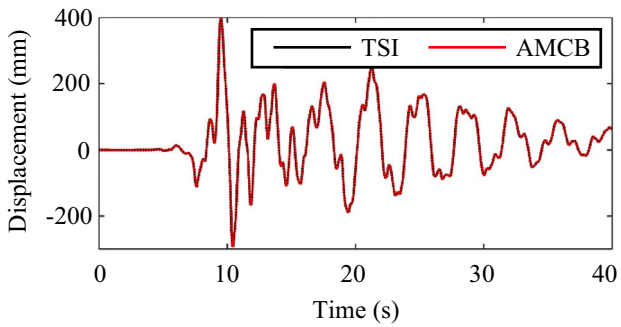

Fig. 15 Roof displacements: *AMCB* adaptive modified Craig-Bampton; *TSI* time step integration [77]

response of large structural components in the medium frequency range. This method has been applied to the dynamic response analysis of the modern satellite SSTL 300 S1.

2.2.2 Free Interface Component Mode Synthesis Method

It is noted from the fixed interface component mode synthesis method that although the DOFs of the FE model are reduced significantly, they highly depend on the DOFs of the interface. To solve this problem, in the late 1960s, Hou [67] and Goldman [81] proposed a free interface component mode synthesis method almost at the same time. However, this method completely ignores the influence of higher-order truncated modes, and the convergence and accuracy of the results are relatively poor. In 1971, MacNeal [68] obtained the first-order approximate residual flexibility of the substructure through the static equilibrium relationship and used the residual flexibility to approximate the influence of higher-order modes on the dynamic characteristics

of the substructure. In 1975, Rubin [69] improved the MacNeal method and introduced the concept of residual inertia on the basis of residual flexibility to obtain the second-order approximate residual flexibility to correct the influence of higher-order truncated modes. In 1976, Craig and Chang [13] further improved the free-interface method, pointed out that the residual flexibility can be used as a Ritz vector, and proposed that the interface force of the substructure can be used as generalized coordinates and be eliminated by the coordination condition of interface force, so as to greatly reduce the final DOFs. This is the free interface method often applied today.

Also taking the structure composed of two substructures as an example, the equation of motion is

$$\begin{bmatrix} \boldsymbol{M}_{II} & \boldsymbol{M}_{IB} \\ \boldsymbol{M}_{BI} & \boldsymbol{M}_{BB} \end{bmatrix} \begin{Bmatrix} \ddot{\boldsymbol{u}}_I \\ \ddot{\boldsymbol{u}}_B \end{Bmatrix} + \begin{bmatrix} \boldsymbol{K}_{II} & \boldsymbol{K}_{IB} \\ \boldsymbol{K}_{BI} & \boldsymbol{K}_{BB} \end{bmatrix} \begin{Bmatrix} \boldsymbol{u}_I \\ \boldsymbol{u}_B \end{Bmatrix} = \begin{Bmatrix} \boldsymbol{0} \\ \boldsymbol{F}_B \end{Bmatrix} \tag{41}$$

where $\boldsymbol{F}_B$ is the force on the interface. For the free interface method, $\boldsymbol{u}_B = 0$ is no longer valid. Therefore, the eigenvalue problem for the overall DOFs of the substructure should be solved. Similar to the fixed interface method, to reduce the model, the higher-order modes are truncated. However, in the free interface method, the influence of higher-order modes is approximated by the residual flexibility. Thus, the first transformation matrix can be expressed by

$$\boldsymbol{\Phi}_f = \left\{ \boldsymbol{\varphi}_N^L \ \boldsymbol{\Psi} \right\} = \begin{bmatrix} \boldsymbol{\varphi}_{NI}^L & \boldsymbol{\Psi}_I \\ \boldsymbol{\varphi}_{NB}^L & \boldsymbol{\Psi}_B \end{bmatrix} \tag{42}$$

where $\boldsymbol{\psi}$ is the residual flexibility matrix. As a result, the reduced model after the first transformation is

$$\tilde{\boldsymbol{M}}\ddot{\boldsymbol{P}} + \tilde{\boldsymbol{K}}\boldsymbol{P} = \tilde{\boldsymbol{F}} \tag{43}$$

where $\boldsymbol{P} = \{\boldsymbol{P}_L, \boldsymbol{F}_B\}^{\mathrm{T}}$, in which $\boldsymbol{P}_L$ is the reduced normalized modal coordinate, and force $\boldsymbol{F}_B$ on the interface can be viewed as a generalized coordinate.

The basis of the second transformation is the interface force equilibrium condition $\boldsymbol{F}_{B,1} = -\boldsymbol{F}_{B,2}$. Combining the two substructures, the generalized coordinate becomes

$$\begin{Bmatrix} \boldsymbol{P}_{L,1} \\ \boldsymbol{F}_{B,1} \\ \boldsymbol{P}_{L,2} \\ \boldsymbol{F}_{B,2} \end{Bmatrix} = \begin{bmatrix} \boldsymbol{I} & \boldsymbol{0} & \boldsymbol{0} \\ \boldsymbol{0} & \boldsymbol{0} & \boldsymbol{I} \\ \boldsymbol{0} & \boldsymbol{I} & \boldsymbol{0} \\ \boldsymbol{0} & \boldsymbol{0} & -\boldsymbol{\mathrm{I}} \end{bmatrix} \begin{Bmatrix} \boldsymbol{P}_{L,1} \\ \boldsymbol{P}_{L,2} \\ \boldsymbol{F}_{B,1} \end{Bmatrix} = \boldsymbol{T}_{f1} \begin{Bmatrix} \boldsymbol{P}_{L,1} \\ \boldsymbol{P}_{L,2} \\ \boldsymbol{F}_{B,1} \end{Bmatrix} \tag{44}$$

According to the first transformation given by Eq. (42), in each substructure, the boundary displacements are

$$\begin{cases} \boldsymbol{u}_{B,1} = \boldsymbol{\varphi}_{NB,1}^L \boldsymbol{P}_{L,1} + \boldsymbol{\psi}_{B,1} \boldsymbol{F}_{B,1} \\ \boldsymbol{u}_{B,2} = \boldsymbol{\varphi}_{NB,2}^L \boldsymbol{P}_{L,2} + \boldsymbol{\psi}_{B,2} \boldsymbol{F}_{B,2} \end{cases} \tag{45}$$

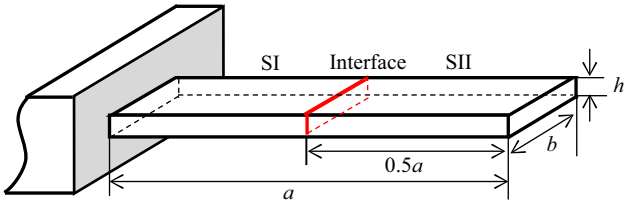

Fig. 16 Schematic diagram of the cantilever plate with two substructures

where $\boldsymbol{u}_{B,1}$ should be equal to $\boldsymbol{u}_{B,2}$ according to the displacement compatibility condition. As a result, the relationship between the interface force $\boldsymbol{F}_B$ and the reserved modal coordinate $\boldsymbol{P}_L$ can be obtained as

$$\begin{aligned} \boldsymbol{F}_{B,1} &= -\boldsymbol{F}_{B,2} \\ &= (\boldsymbol{\Psi}_{B,1} + \boldsymbol{\Psi}_{B,2})^{-1} \left\{ -\boldsymbol{\varphi}_{NB,1}^L \ \ \boldsymbol{\varphi}_{NB,2}^L \right\} \begin{Bmatrix} \boldsymbol{P}_{L,1} \\ \boldsymbol{P}_{L,2} \end{Bmatrix} \\ &= \boldsymbol{L}_1^{-1} \boldsymbol{L}_2 \begin{Bmatrix} \boldsymbol{P}_{L,1} \\ \boldsymbol{P}_{L,2} \end{Bmatrix} \end{aligned} \tag{46}$$

based on which, the generalized coordinate can be rewritten as

$$\begin{Bmatrix} \boldsymbol{P}_{L,1} \\ \boldsymbol{P}_{L,2} \\ \boldsymbol{F}_{B,1} \end{Bmatrix} = \begin{Bmatrix} \boldsymbol{I}_{2k \times 2k} \\ \boldsymbol{L}_1^{-1} \boldsymbol{L}_2 \end{Bmatrix} \begin{Bmatrix} \boldsymbol{P}_{L,1} \\ \boldsymbol{P}_{L,2} \end{Bmatrix} = \boldsymbol{T}_{f2} \begin{Bmatrix} \boldsymbol{P}_{L,1} \\ \boldsymbol{P}_{L,2} \end{Bmatrix} \tag{47}$$

where $\boldsymbol{T}_{f2}$ is the second transformation matrix.

It can be noted from Eq. (47) that the DOFs of the reduced model for the whole structure depend only on the lower-order modes selected in the first transformation, and the interface DOFs are eliminated, which can significantly reduce the dimension of the matrices compared with the fixed interface method. To make the comparison more clearly, an example of a cantilever plate with two substructures are given, as shown in Fig. 16. The natural frequencies of the plate computed by the two methods are shown in Table 2. In the calculation, $a = 0.4$ m, $b = 0.2$ m and $h = 0.005$ m. The material properties of the plate are $E = 210$ GPa, $\upsilon = 0.3$, and $\rho = 7300$ kg/m^3. In the fixed interface method, the first two modes are selected for Substructure I, and the first four modes are selected for Substructure II. There are 33 DOFs on the interface. The total DOF in the fixed interface method is $2 + 4 + 33 = 39$, which is much smaller than the dimension (i.e., 600) of the full FE model. As for the free interface method, the total DOF of the reduced model is just 6, while the natural frequencies are in good agreement with those of the fixed interface model.

The free interface method is widely used in different fields [82–88]. Fan et al. [82] applied the free interface method to the wave and the finite element method to reduce the computational cost while maintaining accuracy. Figure 17 shows the

Table 2 Natural frequencies (Hz) of the cantilever plate obtained by different models

Mode number	Full FE model (DOFs = 660)	Fixed interface model (DOFs = 39)	Free interface model (DOFs = 6)
1	27.74	27.76	27.98
2	118.82	119.56	119.54
3	172.54	173.25	173.24
4	386.11	392.03	389.15
5	482.43	486.84	494.20
6	739.25	760.82	760.50

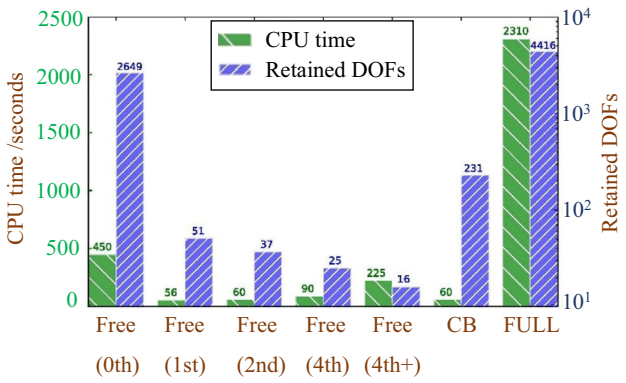

Fig. 17 Efficiency for different models to obtain acceptable results: overall CPU time and retained DOFs, both in the logarithmic scale [82]

calculation cost of different models in the free wave analysis. The results show that the free interface method can greatly reduce the CPU computing time in the free wave analysis.

Folding wings are composed of inner wings and outboard wings. They are widely used in missiles. By extending the connection relationship between the inner wings and the outer wings, Ning et al. [83] established the nonlinear aeroelastic models of folded wing structure by using the free interface method. According to the wind tunnel test results, the flutter characteristics of wings with different freeplay angles were analyzed. The results showed that the free interface method can be used to establish the governing equations and analyze the characteristics of nonlinear aeroelastic systems.

For offshore platforms with excitation load equipment, the fully coupled method is usually used to predict the dynamic characteristics of offshore platforms. However, the calculation cost is relatively high. Based on the free interface method, the dynamic analysis of offshore platform with compressor unit was carried out by Zhao et al. [84]. The results showed that the calculation results of the free interface method and fully coupled method were basically consistent, the calculation time was saved by more than 50%, and the storage space was saved by more than 60%. Li [85] applied the free interface method to the electrostatic analysis of two-dimensional quantum mechanics and calculated the charge concentration and potential distribution of several nanostructures and devices. The results showed that compared with the direct finite element analysis, the free interface method can obtain accurate results and lower calculation cost. Chiello et al. [86] proved that the free interface component mode synthesis technique can effectively solve the structural and acoustic response of elastically-supported baffled plates excited by plane waves or diffuse fields.

Cable vibration in cable-stayed bridges is a very important research field. Based on the free interface method, Chen et al. [87] established a general numerical model of cable net with small DOFs for free and forced vibration analysis. By treating each cable as a substructure and reducing the order, the computational cost was greatly reduced. An example of a cable-stayed bridge verified the effectiveness and accuracy of the method.

The complex eigenvalue analysis is a widely used technique to investigate the stability of a dynamical system with frictional contact. In the case of brake systems, it is the most frequently employed method to study the propensity of the brake to generate squeal noise. However, complex eigenvalue analysis often requires high computational cost. In order to solve this problem, Brizard et al. [88] applied the free interface method in the study of frictional contact. The results showed that the free-interface method can reduce a lot of calculation time.

2.2.3 Mixed Interface Component Mode Synthesis Method

There is a question on how to determine the utilization of the fixed interface method and the free interface method. The case was raised from the literature [89]: if a substructure is very stiff at one interface but relatively flexible at others, the combination of these two methods needs to be used for each of such substructures.

The mixed interface component mode synthesis method is a theory between the fixed interface component mode synthesis method and the free interface component mode synthesis method. This method was first proposed by Benfield and Hruda [14] in 1971, which is also usually called the B-H method. The B-H method does not consider the influence of the slave substructure on the principal modes of the free interface of the master substructure, so the accuracy of the calculation result is not high. In 1985, Jezequel [90] applied dynamic tests and other test methods to obtain the mechanical model of the mixed interface substructure by applying loads on the interface of the substructure. Then he [91] introduced the generalized interface coordinates, further

standardized the mixed interface component mode synthesis method, and qualitatively analyzed the error caused by the truncated higher-order modes. Later, Qiu [92] further improved the mixed interface component mode synthesis method and obtained an accurate mixed interface component mode synthesis method. There are too many branches in the mixed interface component mode synthesis method, but the core ideas of them are almost the same.

The first coordinate transformation of the mixed interface component mode synthesis method is the same as those of the fixed interface method and the free-interface method. The second coordinate transformation should be carried out according to the coordination conditions between different interfaces. It is assumed that the substructure has internal DOFs, fixed interface DOFs, and free interface DOFs at the same time. The equation of motion is

$$\begin{bmatrix} \boldsymbol{M}_{II} & \boldsymbol{M}_{IA} & \boldsymbol{M}_{IC} \\ \boldsymbol{M}_{AI} & \boldsymbol{M}_{AA} & \boldsymbol{M}_{AC} \\ \boldsymbol{M}_{CI} & \boldsymbol{M}_{CA} & \boldsymbol{M}_{CC} \end{bmatrix} \begin{Bmatrix} \ddot{\boldsymbol{u}}_I \\ \ddot{\boldsymbol{u}}_A \\ \ddot{\boldsymbol{u}}_C \end{Bmatrix} + \begin{bmatrix} \boldsymbol{K}_{II} & \boldsymbol{K}_{IA} & \boldsymbol{K}_{IC} \\ \boldsymbol{K}_{AI} & \boldsymbol{K}_{AA} & \boldsymbol{K}_{AC} \\ \boldsymbol{K}_{CI} & \boldsymbol{K}_{CA} & \boldsymbol{K}_{CC} \end{bmatrix} \begin{Bmatrix} \boldsymbol{u}_I \\ \boldsymbol{u}_A \\ \boldsymbol{u}_C \end{Bmatrix} = \begin{Bmatrix} \boldsymbol{0} \\ \boldsymbol{F}_A \\ \boldsymbol{F}_C \end{Bmatrix} \tag{48}$$

where $\boldsymbol{u}_A$ is the DOF of the free interface, $\boldsymbol{u}_C$ is the DOF of the fixed interface, and $\boldsymbol{F}_A$ and $\boldsymbol{F}_C$ are the interface forces. In the mixed interface component mode synthesis method, the assumed mode is composed of three parts as

$$\boldsymbol{\Phi}_m = \begin{bmatrix} \varphi_m^L & \Psi_d & \Psi_c \\ \boldsymbol{0} & \boldsymbol{0} & \boldsymbol{I} \end{bmatrix} = \begin{bmatrix} \varphi_{m,I}^L & \Psi_{d,I} & \Psi_{c,I} \\ \varphi_{m,A}^L & \Psi_{d,A} & \Psi_{c,A} \\ \boldsymbol{0} & \boldsymbol{0} & \boldsymbol{I} \end{bmatrix} \tag{49}$$

where $\boldsymbol{\varphi}_m$ is the mixed interface principal mode. To obtain the normalized mode $\boldsymbol{\varphi}_m$, the eigenvalue problem of the following equation of motion by setting $\boldsymbol{u}_c = 0$ should be solved.

$$\begin{bmatrix} \boldsymbol{M}_{II} & \boldsymbol{M}_{IA} \\ \boldsymbol{M}_{AI} & \boldsymbol{M}_{AA} \end{bmatrix} \begin{Bmatrix} \ddot{\boldsymbol{u}}_I \\ \ddot{\boldsymbol{u}}_A \end{Bmatrix} + \begin{bmatrix} \boldsymbol{K}_{II} & \boldsymbol{K}_{IA} \\ \boldsymbol{K}_{AI} & \boldsymbol{K}_{AA} \end{bmatrix} \begin{Bmatrix} \boldsymbol{u}_I \\ \boldsymbol{u}_A \end{Bmatrix} = \begin{Bmatrix} \boldsymbol{0} \\ \boldsymbol{F}_A \end{Bmatrix} \tag{50}$$

The residual flexibility matrix $\boldsymbol{\psi}_d$ can be obtained by MacNeal's approximation as

$$\boldsymbol{\psi}_d = \left(\begin{bmatrix} \boldsymbol{K}_{II} & \boldsymbol{K}_{IA} \\ \boldsymbol{K}_{AI} & \boldsymbol{K}_{AA} \end{bmatrix}^{-1} - \boldsymbol{\varphi}_m^L \left(\boldsymbol{\Lambda}_m^L \right)^{-1} \left(\boldsymbol{\varphi}_m^L \right)^{\mathrm{T}} \right) \boldsymbol{B}^{\mathrm{T}} \tag{51}$$

where $\boldsymbol{\Lambda}_m^L$ is the eigenvalue corresponding to the mixed-interface main mode $\boldsymbol{\varphi}_m^L$.

In Eq. (49), $\boldsymbol{\psi}_c$ is the constraint mode, which can be obtained by the Guyan method

$$\boldsymbol{\psi}_c = -\begin{bmatrix} \boldsymbol{K}_{II} & \boldsymbol{K}_{IA} \\ \boldsymbol{K}_{AI} & \boldsymbol{K}_{AA} \end{bmatrix}^{-1} \begin{Bmatrix} \boldsymbol{K}_{IC} \\ \boldsymbol{K}_{AC} \end{Bmatrix} \tag{52}$$

Also taking a structure with two substructures as an example, the dynamic equations of the two substructures are combined in the modal coordinate system as

$$\begin{bmatrix} \widehat{\boldsymbol{M}}_1 & \boldsymbol{0} \\ \boldsymbol{0} & \widehat{\boldsymbol{M}}_2 \end{bmatrix} \begin{Bmatrix} \ddot{\boldsymbol{P}}_1 \\ \ddot{\boldsymbol{P}}_2 \end{Bmatrix} + \begin{bmatrix} \widehat{\boldsymbol{K}}_1 & \boldsymbol{0} \\ \boldsymbol{0} & \widehat{\boldsymbol{K}}_2 \end{bmatrix} \begin{Bmatrix} \boldsymbol{P}_1 \\ \boldsymbol{P}_2 \end{Bmatrix} = \begin{Bmatrix} \widehat{\boldsymbol{F}}_1 \\ \widehat{\boldsymbol{F}}_2 \end{Bmatrix} \tag{53}$$

where $\boldsymbol{P} = \{\boldsymbol{P}_I, \boldsymbol{P}_A, \boldsymbol{u}_c\}^{\mathrm{T}}$. The coordination conditions for the generalized coordinate should be

$$\boldsymbol{u}_{A,1} = \boldsymbol{u}_{A,2}, \quad \boldsymbol{P}_{A,1} = -\boldsymbol{P}_{A,2}, \quad \boldsymbol{u}_{C,1} = \boldsymbol{u}_{C,2} \tag{54}$$

based on which, the relationship between different generalized coordinates that is similar to Eq. (46) can be obtained as

$$\begin{aligned} \boldsymbol{P}_{A,1} = -\boldsymbol{P}_{A,2} = & \left(\boldsymbol{\Psi}_{d,A,1} + \boldsymbol{\Psi}_{d,A,2} \right)^{-1} \\ & \cdot \left\{ -\boldsymbol{\varphi}_{m,A,1}^L \quad \boldsymbol{\varphi}_{m,A,2}^L \quad -\boldsymbol{\Psi}_{c,A,1} + \boldsymbol{\Psi}_{c,A,2} \right\} \\ & \cdot \begin{Bmatrix} \boldsymbol{P}_{I,1} \\ \boldsymbol{P}_{I,2} \\ \boldsymbol{u}_C \end{Bmatrix} \end{aligned} \tag{55}$$

As a result, the second transformation matrix is

$$\begin{aligned} \boldsymbol{T}_m = & \begin{bmatrix} \boldsymbol{I} & \boldsymbol{0} & \boldsymbol{0} \\ -\boldsymbol{L}_m \boldsymbol{\varphi}_{m,A,1}^L & \boldsymbol{L}_m \boldsymbol{\varphi}_{m,A,2}^L & \boldsymbol{L}_m \left(-\boldsymbol{\psi}_{c,A,1} + \boldsymbol{\psi}_{c,A,2} \right) \\ \boldsymbol{0} & \boldsymbol{0} & \boldsymbol{I} \\ \boldsymbol{0} & \boldsymbol{I} & \boldsymbol{0} \\ \boldsymbol{L}_m \boldsymbol{\varphi}_{m,A,1}^L & -\boldsymbol{L}_m \boldsymbol{\varphi}_{m,A,2}^L & -\boldsymbol{L}_m \left(-\boldsymbol{\psi}_{c,A,1} + \boldsymbol{\psi}_{c,A,2} \right) \\ \boldsymbol{0} & \boldsymbol{0} & \boldsymbol{I} \end{bmatrix}, \\ \boldsymbol{L}_m = & \left(\boldsymbol{\psi}_{d,A,1} + \boldsymbol{\psi}_{d,A,2} \right)^{-1} \end{aligned} \tag{56}$$

From the above reduced matrices of the overall system, it can be seen that the interface force of the substructure is related not only to the principal mode coordinates but also to the fixed interface DOFs. This method is an organic combination of the fixed interface method and the free interface method. The final reserved DOFs of the system are the principal mode DOFs and fixed interface DOFs. Generally, the number of fixed interface DOFs can be a small quantity, so the number of final system equations can be greatly reduced.

The application of the mixed interface component mode synthesis method is similar to those of the fixed interface method and the free interface method in the engineering field.

Table 3 Summary of advantages, disadvantages and application of DC and CMS methods

		Advantage	Disadvantage	Application
DC	Guyan	Simple	Low accuracy for dynamic problems	1. Damage detection 2. Stochastic FE analysis 3. Model reduction
	Kidder	Applicable for dynamic analysis	Accuracy depends on initial eigenvalues	1. Model reduction
	IRS	High precision	Relatively high computing cost	1. Topology optimization 2. Stochastic FE analysis 3. Damage detection
	SEREP	Allow experiment to match the FE model	The pseudoinverse will cause errors	1. Virtual sensing 2. Update of FE model 3. Damage detection 4. Active control
CMS	Fixed interface	Simple framework	Depends on interface DOFs	1. Product design 2. Damage detection 3. Decentralized control
	Free interface	No interface DOFs	Complex process	1. Free-wave analysis 2. Nonlinear aeroelasticity 3. Model reduction
	Mixed interface	Few interface DOFs	Complex process	1. Model reduction

And because the program of the mixed interface component mode synthesis method is more complex, the mixed interface component mode synthesis method is less used in the engineering field.

2.3 Summary of the DC Method and the CMS Method

In Sects. 2.1 and 2.2, two model reduction techniques, i.e., the dynamic condensation method and the CMS method, have been introduced in detail. In this section, a table (Table 3) is used to briefly summarize the advantages and disadvantages of these two kinds of methods.

3 Some Problems of Dynamic Condensation and CMS Methods

With the wide application of dynamic condensation and CMS methods in the engineering fields, scholars have also found some limitations and problems. Next, the main difficulties encountered are discussed. Some solutions are also proposed.

3.1 Selection Criteria of Master DOFs in Dynamic Condensation

The most important factor affecting the accuracy of dynamic condensation technology is the selection of master DOFs. They determine the matching degree between reduced and full FE models [50]. Therefore, how to choose the master DOFs, and how many master DOFs should be selected are important issues. In the engineering fields, engineers often select the master DOFs based on experience. Unfortunately, for complex structural systems, the determination of master DOFs may not always be obvious. In addition, it is not always reliable to rely on engineers' intuition to select the master DOFs. In order to solve this problem, scholars [93–98] have done a lot of research on the selection of master DOFs and put forward some selection criteria. The specific selection criteria are as follows.

(1) The total number of master DOFs should not be too small and should be at least 2–3 times the number of accurate modes calculated. For inexperienced engineers, the number of master DOFs can be increased to 3.5 times the number of accurate modes, which can reduce the error caused by the improper selection of master DOFs.
(2) According to the characteristics of different structures and loads, the master DOFs should be set on the main deformation or vibration position.
(3) The master DOFs should be set on the element nodes with relatively high stiffness and relatively small mass.

Table 4 Frequencies (Hz) reproduced with permission [107]

Mode number	Substructure A	Substructure B	C-B model	Full model	Difference (%)
1	53.767	19.392	10.162	10.156	0.053
2	163.213	64.216	26.435	26.312	0.470
3	214.125	132.634	58.668	53.431	9.802
4	247.779	148.990	111.776	74.330	50.377
5	258.358	188.709	–	–	–
6	321.073	223.086	–	–	–

(4) For axisymmetric models, the master DOFs can be set at a position parallel to the central line.
(5) The master DOFs should be set at the load action position.
(6) The master DOFs should be set at the result response position.
(7) The master DOFs should not be set on the zero point of a certain mode of the structure.
(8) The selection of master DOFs tends to be displacement DOFs rather than rotational DOFs.

In addition, scholars [99–101] have further developed "automatic" selection methods for master DOFs, which are easy to be directly applied to the computer program of dynamic condensation. These methods can automatically select the master DOFs and are widely used in the engineering fields.

It is worth mentioning that the arrangement of sensors in the modal identification experiment is closely related to the selection criteria of master DOFs in dynamic condensation. The two important physical and dynamic characteristics are both represented, i.e., the spatial incompleteness of the described DOFs of a model and the modal incompleteness of the dynamic behavior that the model represents. It is well known that in modal experiments, due to the mass effect, the number of sensors that can be arranged is limited. It is very important to use limited sensors to obtain as much experimental modal information as possible. The selection of master DOFs in dynamic condensation is essentially the same as the arrangement of sensors, i.e., to select limited master DOFs to retain the modal information of the model as much as possible. Therefore, the arrangement of sensors in the experiment can also refer to the selection criteria of master DOFs in dynamic condensation.

3.2 Interface DOF Reduction and Mode Selection Criteria of the C–B Method

It must be emphasized that, in the C-B method, the final dimension of the reduced model depends greatly on the interface DOFs. Therefore, when the structure scale is very large and complex, it will lead to a very large number of interface DOFs between substructures. In order to solve this defect of the Craig-Bampton method, Craig and Chang [102] proposed three methods to reduce the interface DOFs between substructures, namely, the main mode coordinate reduction, the Guyan reduction, and the improved Ritz reduction. Castanier et al. [103] developed the system-level characteristic constraint (S-CC) mode method, which can reduce the DOFs of the interface before assembling the substructure model. Hong et al. [104] proposed an interface reduction technology, which uses local-level characteristic constraint (L-CC) modes to reduce the DOFs of the interface. Another interface-reduction technique is reported in [105], where the Guyan mode is replaced by the mode computed with fixed-interface neighbors. The interface-reduction methods significantly broaden the application range of the Craig-Bampton method.

In addition, Kuether et al. [106] proposed a selection criterion for the fixed interface modes of substructure. If the accuracy of the frequency band of interest is to be ensured, it is necessary to select at least all fixed interface modes of substructure within 1.5–2 times the maximum frequency of interest. Taking Ref. [107] as an example to explain this selection criterion, in which the natural frequency of the overall structure within 0–30 Hz needs to be calculated, the structure is divided into two substructures, and the natural frequencies of the two substructures under fixed interface are given in Table 4. According to the selection criterion, the fixed interface modes of the substructures should be selected up to 60 Hz. That is to say, the first mode of Substructure I and the first two modes of Substructure II should be selected. The comparison between the natural frequencies obtained by different models is shown in Table 4. It can be seen from the table that within 30 Hz, the natural frequencies obtained by the C-B method are accurate; while beyond the interested range of frequency, the error increases seriously.

3.3 Data Recovery Technologies

As mentioned earlier, when there are many high-order components in the practical vibration, the calculation accuracy of the MD method will be reduced. Therefore, scholars have developed high-precision data recovery technologies, i.e., the

mode acceleration (MA) method and the modal truncation augmentation (MTA) method.

In order to improve the accuracy of substructure data recovery technologies, the influence of higher-order truncated modes needs to be considered. The MA method [71] reduces the influence of high-order truncated modes by adding a static correction to the MD method. According to the first row of Eq. (27), the internal displacement $\boldsymbol{u}_I$ can be obtained as

$$\boldsymbol{u}_I = -\boldsymbol{K}_{II}^{-1}\boldsymbol{M}_{IB}\ddot{\boldsymbol{u}}_B - \boldsymbol{K}_{II}^{-1}\boldsymbol{M}_{II}\ddot{\boldsymbol{u}}_I - \boldsymbol{K}_{II}^{-1}\boldsymbol{K}_{IB}\boldsymbol{u}_B + \boldsymbol{K}_{II}^{-1}\boldsymbol{F}_I \tag{57}$$

Based on the MD recovery, the internal displacement can be expressed by

$$\boldsymbol{u}_I^{MD} = \boldsymbol{\varphi}_{II}^{L}\boldsymbol{x}_N + \boldsymbol{\varphi}_{IB}\boldsymbol{u}_B \tag{58}$$

from which, the internal acceleration can be computed as

$$\ddot{\boldsymbol{u}}_I = \boldsymbol{\varphi}_{II}^{L}\ddot{\boldsymbol{x}}_N + \boldsymbol{\varphi}_{IB}\ddot{\boldsymbol{u}}_B \tag{59}$$

Solving the first line of Eq. (34) by means of Eq. (33), the modal accelerations can be obtained as

$$\ddot{\boldsymbol{x}}_N = \left(\boldsymbol{\varphi}_{II}^{L}\right)^{\mathrm{T}}\boldsymbol{F}_I - \left(\boldsymbol{\varphi}_{II}^{L}\right)^{\mathrm{T}}(\boldsymbol{M}_{IB} + \boldsymbol{M}_{II}\boldsymbol{\varphi}_{IB})\ddot{\boldsymbol{u}}_B - \boldsymbol{\Lambda}_{II}\boldsymbol{x}_N \tag{60}$$

Substitution of Eq. (60) into Eq. (59) gives

$$\begin{aligned}\ddot{\boldsymbol{u}}_I = {} & \boldsymbol{\varphi}_{II}^{L}\left(\boldsymbol{\varphi}_{II}^{L}\right)^{\mathrm{T}}\boldsymbol{F}_I - \boldsymbol{\varphi}_{II}^{L}\left(\boldsymbol{\varphi}_{II}^{L}\right)^{\mathrm{T}}(\boldsymbol{M}_{IB} + \boldsymbol{M}_{II}\boldsymbol{\varphi}_{IB})\ddot{\boldsymbol{u}}_B \\ & - \boldsymbol{\varphi}_{II}^{L}\boldsymbol{\Lambda}_{II}\boldsymbol{x}_N + \boldsymbol{\varphi}_{IB}\ddot{\boldsymbol{u}}_B\end{aligned} \tag{61}$$

which is then substituted into Eq. (57), and the internal displacement by the MA method can be obtained as

$$\boldsymbol{u}_I^{MA} = \boldsymbol{u}_I^{MD} + \boldsymbol{G}_d\left[\boldsymbol{F}_I - \left(\boldsymbol{M}_{IB} - \boldsymbol{M}_{II}\boldsymbol{K}_{II}^{-1}\boldsymbol{K}_{IB}\right)\ddot{\boldsymbol{u}}_B\right] \tag{62}$$

where the residual flexibility matrix of the truncated modes $\boldsymbol{G}_d$ is given by

$$\boldsymbol{G}_d = \boldsymbol{K}_{II}^{-1} - \boldsymbol{\varphi}_{II}^{L}\boldsymbol{\Lambda}_{II}^{-1}\left(\boldsymbol{\varphi}_{II}^{L}\right)^{\mathrm{T}} \tag{63}$$

The MA method has become the most widely used data recovery technology because of its simple program and high precision. In addition, a new data recovery technology, the MTA [108] method, was proposed in 1997. This method supplements the C-B constraint modes and the fixed-interface modes with a set of pseudo eigenvectors. The accuracy of the MTA method is very high, but it requires additional computational effort to calculate the pseudo eigenvectors.

3.4 High-Order Residual Modes (Residual Flexibility) of Free Interface Method

In Hou's method, the influences of the higher-order modes of the substructure are completely ignored, resulting in unacceptable accuracy and computational efficiency of the method. The reasonable construction of higher-order residual modes (residual flexibility) can reduce the calculation error caused by the truncation of higher-order modes and accelerate the convergence speed.

In order to take into account the residual higher-order modes, MacNeal [68] introduced the concept of first-order approximate residual flexibility. If the steady-state response of the substructure is considered, Eq. (41) can be expressed by

$$\boldsymbol{K}\overline{\boldsymbol{u}} = \boldsymbol{F} + \omega^2\boldsymbol{M}\overline{\boldsymbol{u}} \tag{64}$$

where $\overline{\boldsymbol{u}}$ is the amplitude of $\boldsymbol{u}$. In the above equation, if the influence of inertial force is neglected, the first-order approximation of $\overline{\boldsymbol{u}}$ can be obtained as

$${}^{1}\overline{\boldsymbol{u}} = \boldsymbol{K}^{-1}\boldsymbol{F} = \boldsymbol{G}\boldsymbol{F} = \left(\boldsymbol{G}_L + {}^{1}\boldsymbol{G}_d\right)\boldsymbol{F} \tag{65}$$

where the left superscript "1" indicates the first-order approximation, $\boldsymbol{G}$ is the flexibility matrix of substructure, and $\boldsymbol{G}_L$ is the flexibility matrix corresponding to the lower-order reserved mode that can be computed by

$$\boldsymbol{G}_L = \boldsymbol{\varphi}_N^{L}\boldsymbol{\Lambda}_L^{-1}\left(\boldsymbol{\varphi}_N^{L}\right)^{\mathrm{T}},\ {}^{1}\boldsymbol{G}_d = \boldsymbol{G} - \boldsymbol{G}_L = \boldsymbol{K}^{-1} - \boldsymbol{\varphi}_N^{L}\boldsymbol{\Lambda}_L^{-1}\left(\boldsymbol{\varphi}_N^{L}\right)^{\mathrm{T}} \tag{66}$$

which, actually, is the residual flexibility matrix used in the MA method.

Then, the residual mode expression of MacNeal approximation is

$${}^{1}\boldsymbol{\Psi} = {}^{1}\boldsymbol{G}_r\boldsymbol{B}^{\mathrm{T}} = \left[\boldsymbol{K}^{-1} - \boldsymbol{\varphi}_N^{L}\boldsymbol{\Lambda}_L^{-1}\left(\boldsymbol{\varphi}_N^{L}\right)^{\mathrm{T}}\right]\boldsymbol{B}^{\mathrm{T}} \tag{67}$$

Rubin [69] considered the dynamic influence and obtained the second-order approximation of the vibration amplitude by using the results of the first-order approximation as

$${}^{2}\overline{\boldsymbol{u}} = \boldsymbol{G}\left(\boldsymbol{F} + \omega^2\boldsymbol{M}{}^{1}\overline{\boldsymbol{u}}\right) = \boldsymbol{G}\left(\boldsymbol{I} + \omega^2\boldsymbol{M}\boldsymbol{G}\right)\boldsymbol{F} \tag{68}$$

Considering the dynamic influence, the contribution of the lower-order reserved modes of the substructure to the response is

$$^{2}\overline{\boldsymbol{u}}_L = \boldsymbol{G}_L\left(\boldsymbol{I} + \omega^2\boldsymbol{M}\boldsymbol{G}\right)\boldsymbol{F} \tag{69}$$

based on which, the second-order approximation of the residual flexibility matrix is

$$^{2}\boldsymbol{G}_d = (\boldsymbol{G} - \boldsymbol{G}_L)\left(\boldsymbol{I} + \omega^2\boldsymbol{M}\boldsymbol{G}\right) \tag{70}$$

As a result, Rubin's second-order approximation of the residual mode is

$$^{2}\boldsymbol{\Psi} = {}^{2}\boldsymbol{G}_d\boldsymbol{B}^{\mathrm{T}} = (\boldsymbol{G} - \boldsymbol{G}_L)\left(\boldsymbol{I} + \omega^2\boldsymbol{M}\boldsymbol{G}\right)\boldsymbol{B}^{\mathrm{T}} \tag{71}$$

Qiu et al. [109] derived the exact residual mode expression of undamped system using the analytical method. It is composed of the first-order, second-order and higher-order approximations of residual modes as

$$\boldsymbol{\Psi}_q = \boldsymbol{\Psi}_1 + \omega^2\boldsymbol{\Psi}_2 + \omega^4\boldsymbol{\Psi}_3 \tag{72}$$

where $\boldsymbol{\psi}_1$ is the first-order residual mode in MacNeal's approximation, $\boldsymbol{\psi}_1 + \omega^2\boldsymbol{\psi}_2$ is the second-order residual mode in Rubin's approximation, and $\omega^4\boldsymbol{\psi}_3$ is the remaining term of the exact residual term of Rubin' s approximation [110].

Although the approximation methods from Qiu and Rubin have higher accuracy than the first-order approximation method from MacNeal's method, the synthesis equation derived by the exact residual mode and Rubin's approximation contains nonlinear terms, which makes the calculation more complex. The synthesis equation obtained by MacNeal's approximation is linear, and the calculation accuracy can fully meet the engineering needs. Therefore, in practical application, the free interface method generally adopts MacNeal's approximation.

3.5 Rigid Body Mode of Free Interface Method

It should be noted that in Eq. (67), the residual mode of the substructure requires the inverse of its stiffness matrix. The stiffness matrix of the free substructure with rigid body mode is a singular matrix and cannot be inversed. For this case, there are two common treatment methods. The first one is to use the inertia relief attachment mode as the approximation of the truncated high-order mode of the substructure. This method has high calculation accuracy, but the calculation process is relatively complex, so it is less used. The second one is the frequency shifting technique [111], with which the singularity of the stiffness matrix of the substructure is eliminate, and the residual modes of the substructure are still used to approximate the truncated high-order modes. The basic formula of the frequency shifting technique is

$$\boldsymbol{K}_f = \boldsymbol{K} + \alpha\boldsymbol{M} \tag{73}$$

where $\boldsymbol{K}_f$ is the stiffness matrix after the frequency shift; $\boldsymbol{K}$ and $\boldsymbol{M}$ are the stiffness matrix and mass matrix before the frequency shift, respectively; and α is the amount of frequency shift. After the frequency shift treatment, the mode shape of the structure does not change. The correct eigenvalue can be obtained by subtracting the amount of frequency shift from the eigenvalue after the frequency shift. It can be seen from the characteristics of the frequency shift method that whether the structure has rigid body mode or not, the frequency shift treatment will not affect its dynamic characteristics, which provides a theoretical basis for the application of the frequency shift technology in the free-interface method.

When a free substructure in the system needs frequency shift, other substructures must also have frequency shifts with the same amount. The determination of the frequency shift amount is generally by experience. When the frequency shift amount is much larger than the low-order frequency of the structure, due to the influence of the computer's effective word length and rounding error, the large number operation will cause large errors and even lead to wrong calculation results. Therefore, the frequency shift amount should not be too large. At present, some scholars [112–114] have studied the amount of frequency shift and obtained some conclusions. In general, taking the square of the lower-order mode frequency as the frequency shift amount can eliminate the singularity of the stiffness matrix and ensure better accuracy.

3.6 Non-classical Damping System CMS Method

The above CMS methods are usually for undamped structures or structures with proportional damping. Although these methods have achieved great success in subsequent engineering applications, the actual structures are usually damped and often do not accord with the proportional damping assumption. In particular, composite materials are widely used in modern engineering structures, resulting in the above CMS methods gradually showing their limitations. Therefore, the research of the CMS method for non-classical damping structures has attracted more and more attention and become the development trend of the modern CMS method.

For non-classical damped structures, it is usually necessary to transform their physical equations into state space and establish the modal base of substructures by solving their complex modes. Craig and Bampton [12] first proposed the CMS method for non-classical damping systems in 1968. Hasselman and Kaplan [115] improved on the basis of [12] and compensated the response of high-order truncated complex modes by defining generalized additional residual modes. Considering the influence of residual modes, Craig and Chung [116] proposed a free interface complex mode method for non-classical damped structures. Some scholars have also improved the mode truncation method of the

non-classical damping CMS method in calculation accuracy, including the first-order approximation method which only considers the inertia-relief modes of subcomponents [117–120] and the second-order approximation method taking both static flexibility and dynamic effects of truncated modes into account [121, 122].

The above methods are based on the complex modal analysis of non-classical damped structures by transforming the vibration equation from physical space to state space, and then use the obtained complex modes for modal synthesis. However, this will double the dimensions of the undamped system. In order to solve this limitation, Xiang et al. [123] constructed the modal subspace by using the Schur vector instead of the complex mode for modal synthesis, which completely avoids the complex modal analysis and improves the calculation efficiency. However, unlike the complex mode, the Schur vector cannot describe the modal characteristics of general damping structures in the physical sense, which limits its application. By introducing the residual static vector related to an external load and viscoelastic damping force, De Lima et al. [124] improved the classical C-B method and extended it to a large-scale viscoelastic damping system. Taking the aeronautical engineering structure as an example, the effectiveness of this method for complex viscoelastic structures is verified. By introducing residual attachment modes of the system matrix, Li and Hu [111] proposed a model reduction method of a viscoelastic damping system based on the free interface CMS method. The accuracy and effectiveness of the proposed method are verified by numerical calculation. The CMS method of the above non-classical damping system makes up for the defects of the traditional CMS method.

3.7 Model Reduction Methods for Geometrically Nonlinear Structures

Thin structures, such as beams, plates, and shells, will generate large-amplitude vibration with geometric nonlinearity due to their relatively low bending stiffness. Geometric nonlinearity, in terms of its nature, is a kind of distributed nonlinearity, which means that all DOFs of the model are nonlinearly coupled [125]. On the contrary, other types of nonlinearities, such as those related to contact, are related to local nonlinearity. For the latter case, this review has mentioned the application of dynamic condensation and CMS methods. However, these two methods do not perform well in the presence of geometric nonlinearity because they typically do not capture the relevant bending/torsion-stretching coupling [126]. For model reduction of geometrically nonlinear structures, nonlinear mapping methods are usually used, including but not limited to nonlinear regular modes, implicit condensation, quadratic manifolds, spectral submanifolds, direct normal forms, etc. This section will briefly introduce the application of these methods in model reduction of geometrically nonlinear structures.

The nonlinear normal mode is defined as a nonlinear extension of the concept of linear normal mode [127], which provides a strict mathematical and geometric tool for describing the behavior of geometrically nonlinear systems. Based on the nonlinear normal mode method, Kerschen et al. [128] obtained a reduced order nonlinear FE model of Morane-Saulnier Paris aircraft and calculated the nonlinear normal mode of the aircraft. Kuether et al. [129] proposed a method combining reduced-order modeling and numerical continuation to estimate the nonlinear normal modes of geometrically nonlinear FE models and calculated the reduced order model with hardening nonlinearity of the exhaust panel cover structure to prove the speed advantage of the new method. Haller and Ponsioen [130] proposed a unified method for nonlinear modal analysis of dissipative oscillation systems based on the nonlinear normal mode.

Implicit condensation was first proposed by Ewan and Hollkamp [131]. Sometimes it is also called the applied force method because it relies on applying a set of selected static forces on the FE model and constructing a stress manifold as the first step of deriving the reduced order model. Based on implicit condensation, Frangi and Gobat [132] reduced the order of the geometrically nonlinear FE model of softening disk ring gyroscope and studied the influence of nonlinear stiffness in micro-electro-mechanical system resonator. The slow-fast decomposition proposed by Haller and Ponsioen [133] for the first time provides mathematical proof for implicit condensation and quadratic manifold. Shen et al. [134] compared three methods (implicit condensation, quadratic manifold, direct normal form) for model reduction of geometrically nonlinear structures in the general framework of FE programs. The implicit condensation method and quadratic manifold method both require slow-fast assumptions, and they cannot predict the correct nonlinear type when the assumptions are not realized. The direct normal form method has the invariance property embedded without any additional assumptions.

The quadratic manifold method based on modal derivative was first proposed in [126, 135]. The main idea is to derive a nonlinear mapping by using the modal derivatives as a quadratic dependence on the master coordinates to pass from the FE nodes to a reduced subspace built on a quadratic manifold. Jain and Tiso [136] introduced a new method to generate training sets for hyper-reduction of geometrically nonlinear structural dynamics problems without the need for full solution snapshots, thus greatly reducing the computational cost of the quadratic manifold method. The example shows that the effective speed-up value of the method in the literature [136] is 44.38, while that of the classical method is 0.73 (The higher is the effective speed-up value, the more favorable is the given reduction method). Vizzaccaro et al.

[137] compared the application of two nonlinear mapping methods (the normal form theory and the quadratic manifold method with modal derivatives) in reducing the order of geometrically nonlinear models. The investigation results show that only when the slow/fast assumption between master and slave coordinates is true, the results predicted by the quadratic manifold method with modal derivatives converge to those provided by the normal form theory. This result completely conforms to the general theorem provided in [133].

The spectral submanifold was first proposed by Haller and Ponsioen [130] in 2016. The spectral submanifold is an invariant manifold asymptotic to the nonlinear regular mode and the smoothest nonlinear continuation of the spectral subspace of a linearized system along the nonlinear regular mode. Based on the theory of spectral submanifold, Li et al. [138, 139] constructed a reduced-order model of harmonically excited mechanical systems with internal resonance. The periodic response and quasi-periodic responses of the structure were calculated using the reduced order model. Cenedese et al. [140] developed a data-driven nonlinear model reduction method based on spectral submanifolds and applied it to geometrically nonlinear mechanical systems.

The direct normal form method was proposed [141] in 2021, which allows direct calculation of nonlinear mapping and enables one to pass from the FE DOFs to the invariant manifold of the system tangent to the linear counterpart of the origin. This method bypasses the steps of eigenmode projection, so it is suitable for order reduction of large geometrically nonlinear models (millions of DOFs). Opreni et al. [142] reduced the geometrically nonlinear FE model of large micro-electro-mechanical structures with internal resonance based on the direct normal form method.

It is worth noting that the advantage of the direct normal form method is that its ROMs is explicit, and the implementation in [141] is non-intrusive (without the need to enter new calculations at the elementary level in the code). However, the direct normal form method can only assume proportional damping and is limited to nonlinear problems related to the quadratic and cubic displacement [134, 141, 142], so the results will deteriorate at very large amplitudes. In contrast, the model reduction based on spectral submanifold is suitable for general dynamic systems [130, 138–140], even for systems with asymmetric damping and stiffness matrices [143] and configuration constraints. Li et al. [143] reduced the nonlinear model with asymmetric damping and stiffness matrix (a cantilever pipe conveying fluid) based on the spectral submanifold. In addition, in Jain and Haller's latest research [144], a calculation method for automated construction of spectral submanifold was proposed, which bypasses the step of calculating all eigenmodes (writing equations of motion in modal coordinates). Therefore, the spectral submanifold method is also suitable for order reduction of large geometrically nonlinear models.

3.8 Interface Coupling Mechanism of Substructure in CMS Method

The second coordinate transformation in the CMS method is obtained by assuming that the substructure is completely fixed. However, the common connection methods (bolted connection, riveting, etc.) in engineering structures usually do not meet the assumption of completely fixed connection, which will lead to an incorrect estimation of the stiffness of the reduced order model. An interface coupling mechanism of the free interface method for elastic connection conditions was proposed in the literature [83]. When the substructure is elastically connected, the interface coordination condition of the free interface method is $\boldsymbol{F}_{B,1} = -\boldsymbol{F}_{B,2}$ and $\boldsymbol{u}_{B,1} = \boldsymbol{u}_{B,2} + \boldsymbol{\delta}$. Therefore, Eq. (45) can be rewritten as

$$\boldsymbol{\varphi}_{NB,1}^{L}\boldsymbol{P}_{L,1} + \boldsymbol{\Psi}_{B,1}\boldsymbol{F}_{B,1} = \boldsymbol{\varphi}_{NB,2}^{L}\boldsymbol{P}_{L,2} + \boldsymbol{\Psi}_{B,2}\boldsymbol{F}_{B,2} + \boldsymbol{\delta} \tag{74}$$

where $\boldsymbol{\delta}$ is the relative displacement. The internal force can be expressed by the parameter $\boldsymbol{\delta}$. Equation (46) can be rewritten as

$$\begin{aligned}\boldsymbol{F}_{B,1} &= -\boldsymbol{F}_{B,2} \\ &= \left(\boldsymbol{\Psi}_{B,1} + \boldsymbol{\Psi}_{B,2}\right)^{-1}\left\{-\boldsymbol{\varphi}_{NB,1}^{L}\ \boldsymbol{\varphi}_{NB,2}^{L}\ \boldsymbol{I}\right\}\begin{Bmatrix}\boldsymbol{P}_{L,1}\\ \boldsymbol{P}_{L,2}\\ \boldsymbol{\delta}\end{Bmatrix} \\ &= \boldsymbol{L}_1^{-1}\tilde{\boldsymbol{L}}_2\begin{Bmatrix}\boldsymbol{P}_{L,1}\\ \boldsymbol{P}_{L,2}\\ \boldsymbol{\delta}\end{Bmatrix}\end{aligned} \tag{75}$$

Therefore, the second transformation matrix can be obtained as

$$\tilde{\boldsymbol{T}}_f = \begin{bmatrix}\boldsymbol{I} & \boldsymbol{0} & \boldsymbol{0}\\ -\boldsymbol{L}_1^{-1}\boldsymbol{\varphi}_{NB,1}^{L} & \boldsymbol{L}_1^{-1}\boldsymbol{\varphi}_{NB,2}^{L} & \boldsymbol{L}_1^{-1}\\ \boldsymbol{0} & \boldsymbol{I} & \boldsymbol{0}\\ \boldsymbol{L}_1^{-1}\boldsymbol{\varphi}_{NB,1}^{L} & -\boldsymbol{L}_1^{-1}\boldsymbol{\varphi}_{NB,2}^{L} & -\boldsymbol{L}_1^{-1}\end{bmatrix} \tag{76}$$

based on which, one can have

$$\begin{aligned}&\tilde{\boldsymbol{T}}_f^{\mathrm{T}}\begin{bmatrix}\tilde{\boldsymbol{M}}_1 & \boldsymbol{0}\\ \boldsymbol{0} & \tilde{\boldsymbol{M}}_2\end{bmatrix}\tilde{\boldsymbol{T}}_f\begin{Bmatrix}\ddot{\boldsymbol{P}}_{L,1}\\ \ddot{\boldsymbol{P}}_{L,2}\\ \ddot{\boldsymbol{\delta}}\end{Bmatrix} \\ &+\tilde{\boldsymbol{T}}_f^{\mathrm{T}}\begin{bmatrix}\tilde{\boldsymbol{K}}_1 & \boldsymbol{0}\\ \boldsymbol{0} & \tilde{\boldsymbol{K}}_2\end{bmatrix}\tilde{\boldsymbol{T}}_f\begin{Bmatrix}\boldsymbol{P}_{L,1}\\ \boldsymbol{P}_{L,2}\\ \boldsymbol{\delta}\end{Bmatrix} = \tilde{\boldsymbol{T}}_f^{\mathrm{T}}\begin{Bmatrix}\boldsymbol{\varphi}_{NB,1}^{L}\boldsymbol{F}_{B,1}\\ \boldsymbol{\Psi}_{B,1}\boldsymbol{F}_{B,1}\\ \boldsymbol{\varphi}_{NB,2}^{L}\boldsymbol{F}_{B,2}\\ \boldsymbol{\Psi}_{B,2}\boldsymbol{F}_{B,2}\end{Bmatrix}\end{aligned} \tag{77}$$

It is noted that, the generalized force related to the generalized coordinate $\boldsymbol{\delta}$ is

$$\begin{aligned}&\boldsymbol{L}_1^{-1}\boldsymbol{\Psi}_{B,1}\boldsymbol{F}_{B,1}-\boldsymbol{L}_1^{-1}\boldsymbol{\psi}_{B,2}\boldsymbol{F}_{B,2}\\&\quad=-\boldsymbol{L}_1^{-1}\left(\boldsymbol{\Psi}_{B,1}+\boldsymbol{\Psi}_{B,2}\right)\boldsymbol{F}_{B,2}=-\boldsymbol{F}_{B,2}\end{aligned}\tag{78}$$

which is then substituted into Eq. (77), the generalized force related to generalized coordinate $\boldsymbol{\delta}$ is retained, and the elastic connected force is considered by

$$\begin{aligned}&\tilde{\boldsymbol{T}}_f^{\mathrm{T}}\begin{bmatrix}\tilde{\boldsymbol{M}}_1 & \boldsymbol{0}\\ \boldsymbol{0} & \tilde{\boldsymbol{M}}_2\end{bmatrix}\tilde{\boldsymbol{T}}_f\begin{Bmatrix}\ddot{\boldsymbol{P}}_{L,1}\\ \ddot{\boldsymbol{P}}_{L,2}\\ \ddot{\boldsymbol{\delta}}\end{Bmatrix}\\&+\tilde{\boldsymbol{T}}_f^{\mathrm{T}}\begin{bmatrix}\tilde{\boldsymbol{K}}_1 & \boldsymbol{0}\\ \boldsymbol{0} & \tilde{\boldsymbol{K}}_2\end{bmatrix}\tilde{\boldsymbol{T}}_f\begin{Bmatrix}\boldsymbol{P}_{L,1}\\ \boldsymbol{P}_{L,2}\\ \boldsymbol{\delta}\end{Bmatrix}+\begin{Bmatrix}\boldsymbol{0}\\ \boldsymbol{0}\\ \boldsymbol{F}_{B,2}\end{Bmatrix}=\boldsymbol{0}\end{aligned}\tag{79}$$

In general, the internal force is related to the relative displacement $\boldsymbol{\delta}$. For linear case, the generalized force is the product of the generalized displacements and the linear stiffness, that is, $\boldsymbol{F}_{B,2}=\boldsymbol{k}_{\mathrm{e}}\boldsymbol{\delta}$, where $\boldsymbol{k}_{\mathrm{e}}$ is the linear stiffness. As a result, Eq. (79) can be further written as

$$\begin{aligned}&\tilde{\boldsymbol{T}}_f^{\mathrm{T}}\begin{bmatrix}\tilde{\boldsymbol{M}}_1 & \boldsymbol{0}\\ \boldsymbol{0} & \tilde{\boldsymbol{M}}_2\end{bmatrix}\tilde{\boldsymbol{T}}_f\begin{Bmatrix}\ddot{\boldsymbol{P}}_{L,1}\\ \ddot{\boldsymbol{P}}_{L,2}\\ \ddot{\boldsymbol{\delta}}\end{Bmatrix}\\&+\left(\tilde{\boldsymbol{T}}_f^{\mathrm{T}}\begin{bmatrix}\tilde{\boldsymbol{K}}_1 & \boldsymbol{0}\\ \boldsymbol{0} & \tilde{\boldsymbol{K}}_2\end{bmatrix}\tilde{\boldsymbol{T}}_f+\begin{bmatrix}\boldsymbol{0}&\boldsymbol{0}&\boldsymbol{0}\\ \boldsymbol{0}&\boldsymbol{0}&\boldsymbol{0}\\ \boldsymbol{0}&\boldsymbol{0}&\boldsymbol{k}_{\mathrm{e}}\end{bmatrix}\right)\begin{Bmatrix}\boldsymbol{P}_{L,1}\\ \boldsymbol{P}_{L,2}\\ \boldsymbol{\delta}\end{Bmatrix}\\&=\boldsymbol{0}\end{aligned}\tag{80}$$

The above equation shows that various connection methods in engineering structures can be approximately satisfied by arbitrarily adjusting the linear stiffness $\boldsymbol{k}_{\mathrm{e}}$. A similar method was also proposed to deal with the elastic connection between substructures [145]. However, the accuracy of this method is not very high, and the linear stiffness $\boldsymbol{k}_{\mathrm{e}}$ is also difficult to determine. At present, there is little research on this problem, which is also one of the future development trends of the CMS method.

4 Conclusions

In this paper, two main categories of model reduction technology, i.e., dynamic condensation and CMS methods, are reviewed. The historical development, theoretical framework, and the latest application of the two categories of model reduction methods are introduced. Finally, some important open issues of the two categories of methods are discussed. Based on the above review, we believe that some interesting and valuable research needs to be improved and expanded further. Some discussions on the prospects for further research are summarized as follows.

(1) Large dimensional system equations in state space often lead to time delay of active control. Dynamic condensation has good potential in reducing the dimension of system equations. However, there are still few studies on the application of dynamic condensation in active control. It is necessary to study the cooperation between dynamic condensation and active control methods.
(2) The application of the CMS method in multifield problems is introduced above. However, this part of the literature is still limited. Especially in the field of computational fluid dynamics (CFD), high computational cost and hardware cost are common problems. The combination of the CMS method and CFD has great application prospects.
(3) How to correctly create the interface coordination conditions between substructures is another field that needs to be explored in future research. The second coordinate transformation in the CMS method needs to establish the transformation matrix based on the interface displacement coordination. This assumption is more consistent with the case of completely fixed connection between substructures. However, for the common connection methods in engineering, such as bolt, riveting and other connection methods, the classical assumption cannot be accurately analyzed. Therefore, it is necessary to study the interface coordination conditions of various connection methods in practical engineering.
(4) In terms of engineering application, the most promising CMS method should be the mixed interface component mode synthesis method. But so far, the most widely used method is the C-B method. The reason is that the C-B method has a simple program and convenient application. In addition, the mixed interface component mode synthesis method does not have a unified framework recognized by the engineering community. Therefore, developing a recognized and simple unified framework for the mixed interface method has become an urgent problem to be solved.

Acknowledgements The work described in this paper was supported by grants from the National Natural Science Foundation of China (Grant No. 11802069), China Postdoctoral Science Foundation (No. 3236310534), and Heilongjiang Provincial Postdoctoral Science Foundation (No. 002020830603).

References

1. Xia Y, Hao H, Deeks AJ, Zhu XQ. Condition assessment of shear connectors in slab-girder bridges via vibration measurements. J Bridg Eng. 2008;13(1):43–54.
2. Duan YF, Xu YL, Fei QG, Wong KY, Chan KWY, Ni YQ, et al. Advanced finite element model of Tsing Ma bridge for structural health monitoring. Int J Struct Stab Dyn. 2011;11(2):313–44.
3. Ni YQ, Xia Y, Lin W, Chen WH, Ko JM. SHM benchmark for high-rise structures: a reduced-order finite element model and field measurement data. Smart Struct Syst. 2012;10(4–5):411–26.
4. Fan XH, Chen P, Wu RA, Xiao SF. Parallel computing study for the large-scale generalized eigenvalue problems in modal analysis. Sci China-Phys Mech Astron. 2014;57(3):477–89.
5. Fan XH, Wang KY, Xiao SF. Large-scale parallel computation for earthquake response spectrum analysis. Eng Comput. 2018;35(2):800–17.
6. Zhang JQ, Ankit A, Gravenkamp H, Eisentrager S, Song CM. A massively parallel explicit solver for elasto-dynamic problems exploiting octree meshes. Comput Methods Appl Mech Eng. 2021;380: 113811.
7. Daniel T, Casenave F, Akkari N, Ryckelynck D, Rey C. Uncertainty quantification for industrial numerical simulation using dictionaries of reduced order models. Mech Ind. 2022;23:3.
8. Guyan RJ. Reduction of stiffness and mass matrices. AIAA J. 1965;3(2):380.
9. Kidder RL. Reduction of structural frequency equations. AIAA J. 1973;11(6):892.
10. O'Callahan J. A Procedure for an Improved Reduced System (IRS) Model. in: Proceedings of the 7th International Modal analysis conference; 1989, p. 17–21.
11. O'Callahan J. System equivalent reduction and expansion process. Proceedings of the 7th International Modal analysis conference, Society of Experimental Mechanics. 1989;7:29–37.
12. Craig RR, Bampton MCC. Coupling of substructures for dynamic analyses. AIAA J. 1968;6(7):1313–9.
13. Craig RR, Chang CJ. Free-interface methods of substructure coupling for dynamic analysis. AIAA J. 1976;14(11):1633–5.
14. Benfield WA, Hruda RF. Vibration analysis of structures by component mode substitution. AIAA J. 1971;9(7):1255–61.
15. Kim JH, Boo SH, Lee PS. A dynamic condensation method with free interface substructuring. Mech Syst Signal Process. 2019;129:218–34.
16. Yin T, Lam HF, Chow HM, Zhu HP. Dynamic reduction-based structural damage detection of transmission tower utilizing ambient vibration data. Eng Struct. 2009;31(9):2009–19.
17. Kim CW, Kawatani M. Pseudo-static approach for damage identification of bridges based on coupling vibration with a moving vehicle. Struct Infrastruct Eng. 2008;4(5):371–9.
18. Mcgowan P, Angelucci A, Javeed M. Dynamic test/analysis correlation using reduced analytical models. 33rd Structures, Structural Dynamics and Materials Conference; 1992, p.2335.
19. Avitabile P. Model reduction and model expansion and their applications–part 1 theory. Proceedings of the Twenty-Third International Modal Analysis Conference; 2005.
20. Irons B. Eigenvalue economisers in vibration problems. J R Aeronaut Soc. 1963;67:526.
21. Irons B. Structural eigenvalue problems - elimination of unwanted variables. AIAA J. 1965;3(5):961–2.
22. Friswell M, Garvey S, Penny J. Model reduction using dynamic and iterated IRS techniques. J Sound Vib. 1995;186(2):311–23.
23. Friswell M, Garvey S, Penny J. The convergence of the iterated IRS method. J Sound Vib. 1998;211:123–32.
24. Turner MJ, Clough RW, Martin HC, Topp LJ. Stiffness and deflection analysis of complex structures. J Aeronaut Sci. 1956;23(9):805–23.
25. Aglietti GS, Walker SJI, Kiley A. On the use of SEREP for satellite FEM validation. Eng Comput. 2012;29(6):580–95.
26. Hughes TJR. The Finite Element Method: Linear Static and Dynamic Finite Element Analysis. Mineola, NY, USA: Dover; 2000.
27. Kim J-G, Lee P-S. An accurate error estimator for Guyan reduction. Comput Methods Appl Mech Eng. 2014;278:1–19.
28. Kim J-G, Boo S-H, Lee C-O, Lee P-S. On the computational efficiency of the error estimator for Guyan reduction. Comput Methods Appl Mech Eng. 2016;305:759–76.
29. Xia Y, Lin R. A new Iterative Order Reduction (IOR) method for eigensolutions of large structures. Int J Numer Meth Eng. 2004;59(1):153–72.
30. Li H, Wang J, James Hu S-L. Using incomplete modal data for damage detection in offshore jacket structures. Ocean Eng. 2008;35(17–18):1793–9.
31. Yang Y, Mace BR, Kingan MJ. A wave and finite element based homogenised model for predicting sound transmission through honeycomb panels. J Sound Vib. 2019;463: 114963.
32. Panayirci HM, Pradlwarter HJ, Schuëller GI. Efficient stochastic structural analysis using Guyan reduction. Adv Eng Softw. 2011;42(4):187–96.
33. Mercer JF, Aglietti GS, Kiley AM. Model reduction and sensor placement methods for finite element model correlation. AIAA J. 2016;54(12):3941–55.
34. Zhang N, Hu W, Hahn E. Model Reduction of Large Rotor-Bearing-Foundation Systems. in: 51st ASME Turbo Expo, Barcelona, SPAIN: 2006, p. 1331–1340.
35. Dinh-Cong D, Truong TT, Nguyen-Thoi T. A comparative study of different dynamic condensation techniques applied to multi-damage identification of FGM and FG-CNTRC plates. Eng Comput. 2022;38:3951–75.
36. Maia NMM, Silva TAN. An expansion technique for the estimation of unmeasured rotational frequency response functions. Mech Syst Signal Process. 2021;156: 107634.
37. Gordis J. An analysis of the Improved Reduced System (IRS) model reduction procedure. in: Proceedings of the 10th International Modal Analysis Conference, San Diego, USA: 1992, p. 471–479.
38. Friswell M, Garvey S, Penny J. Using Iterated IRS Model Reduction Techniques to Calculate Eigensolutions. Proceedings of SPIE - The International Society for Optical Engineering. in: 15th International Modal Analysis Conference, Orlando, USA: 1997, p. 1537–1543.
39. Kuhar EJ, Stahle CV. Dynamic transformation method for modal synthesis. AIAA J. 1973;12(5):672–8.
40. Blair M, Camino T, Dickens J. An iterative approach to a reduced mass matrix. In: 9th Conference International Modal Analysis Conference (IMAC). 1991, p. 621–626.
41. Friswell M, Penny J, Garvey S. The application of the IRS and balanced realization methods to obtain reduced models of structures with local non-linearities. J Sound Vib. 1996;196:453–68.
42. Zare Hosseinzadeh A, Seyed Razzaghi SA, Ghodrati AG. An iterated IRS technique for cross-sectional damage modelling and identification in beams using limited sensors measurement. Inverse Prob Sci Eng. 2018;27(8):1145–69.
43. Xie Q, Zhang N, Zhang B, Ji J. Boundary condition handling approaches for the model reduction of a vehicle frame. Mech Syst Signal Process. 2016;75:123–37.
44. Ni P, Li J, Hao H, Xia Y. Stochastic dynamic analysis of marine risers considering Gaussian system uncertainties. J Sound Vib. 2018;416:224–43.

45. Kim H-G, Park S-h, Cho M. Structural topology optimization based on system condensation. Finite Elements in Analysis and Design. 2014;92:26–35.
46. Choi D, Kim H, Cho M. Improvement of substructuring reduction technique for large eigenproblems using an efficient dynamic condensation method. J Mech Sci Technol. 2008;22(2):255–68.
47. Chandraker S, Roy H. Dynamic study of viscoelastic rotor: reduction of higher order model using different techniques. Aerosp Sci Technol. 2016;58:306–17.
48. O'Callahan J, Li P. The Effects of Modal Vector Expansion on Finite Element Model Updating. in: 13th International Modal Analysis Conference. Bethel, CT: 1995.
49. Kammer D. Test-analysis model development using an exact modal reduction. Int J Anal Exp Modal Anal. 1987;2:174–9.
50. Bonisoli E, Delprete C, Rosso C. Proposal of a modal-geometrical-based master nodes selection criterion in modal analysis. Mech Syst Signal Process. 2009;23(3):606–20.
51. Ghannadi P, Kourehli SS. Data-driven method of damage detection using sparse sensors installation by SEREPa. J Civ Struct Heal Monit. 2019;9(4):459–75.
52. Sanches FD, Pederiva R. Simultaneous identification of unbalance and shaft bow in a two-disk rotor based on correlation analysis and the SEREP model order reduction method. J Sound Vib. 2018;433:230–47.
53. Das AS, Dutt JK. A reduced rotor model using modified SEREP approach for vibration control of rotors. Mech Syst Signal Process. 2012;26:167–80.
54. Das AS, Dutt JK. Reduced model of a rotor-shaft system using modified SEREP. Mech Res Commun. 2008;35(6):398–407.
55. Ganguly K, Roy H. SEREP-based reduced model of higher order viscoelastic propeller shaft considering various asymmetries. Eng Comput. 2020;37(4):3237–49.
56. Mendonsa CD, Monteiro UA, Gutierrez RHR, Vaz LA, Medeiros J, Tinoco EB. Prediction of vibration responses in a reciprocating compressor interstage piping system using the modal expansion method. The Int J Adv Manuf Technol. 2022;119(5–6):4073–89.
57. Tarpo M, Nabuco B, Georgakis C, Brincker R. Expansion of experimental mode shape from operational modal analysis and virtual sensing for fatigue analysis using the modal expansion method. Int J Fatigue. 2020;130: 105280.
58. Thibault L, Avitabile P, Foley J, Wolfson J. Equivalent reduced model technique development for nonlinear system dynamic response. Mech Syst Signal Process. 2013;36(2):422–55.
59. Lal HP, Jith J, Gupta S, Sarkar S. Reduced order modelling in stochastically parametered acousto-elastic system using arbitrary PCE based SEREP. Probab Eng Mech. 2018;52:1–14.
60. Sarkar S, Venkatraman K. Model order reduction of unsteady flow past oscillating airfoil cascades. J Fluids Struct. 2004;19(2):239–47.
61. Craig RR. A review of time-domain and frequency-domain component mode synthesis method. NASA, 1985.
62. Craig, RR. Coupling of substructures for dynamic analyses - An overview. in: 41st Structures, Structural Dynamics, and Materials Conference and Exhibit: AIAA; 2000, p. 1573.
63. Craig RR, Kurdila AJ. Fundamentals of structural dynamics. Hoboken, USA: John Wiley & Sons; 2006.
64. de Klerk D, Rixen DJ, Voormeeren SN. General framework for dynamic substructuring: history, review and classification of techniques. AIAA J. 2008;46(5):1169–81.
65. Hintz RM. Analytical methods in component modal synthesis. AIAA J. 1975;13(8):1007–16.
66. Hurty WC. Dynamic analysis of structural systems using component modes. AIAA J. 1965;3(4):678–85.
67. Hou SN. Review of modal synthesis techniques and a new approach. Shock Vib Bull. 1969;40:25–39.
68. MacNeal R. A hybrid method of component mode synthesis. Comput Struct. 1971;1:581–601.
69. Rubin S. Improved component-mode representation for structural dynamic analysis. AIAA J. 1975;13:995–1006.
70. Craig RR, Chang CJ. Substructure Coupling for Dynamic Analysis and Testing. In: NASA. CR-2781, 1977.
71. Fransen SHJA. Data recovery methodologies for reduced dynamic substructure models with internal loads. AIAA J. 2004;42(10):2130–42.
72. Vizzini S, Olsson M, Scattina A. Component mode synthesis methods for a body-in-white noise and vibration analysis. Proceedings of the Institution of Mechanical Engineers Part D-Journal of Automobile Engineering. 2017;231(2):279-88.
73. Mahmoudi S, Trivaudey F, Bouhaddi N. Benefits of metamodel-reduction for nonlinear dynamic response analysis of damaged composite structures. Finite Elem Anal Des. 2016;119:1–14.
74. Wagner JL, Bohm M, Sawodny O. Decentralized structural control using Craig-Bampton reduction and local controller design. IEEE International Conference on Industrial Technology (ICIT); 2020 Feb 26–28; Buenos Aires, ARGENTINA, 2020, p. 41–46.
75. Nachtergaele P, Rixen DJ, Steenhoek AM. Efficient weakly coupled projection basis for the reduction of thermo-mechanical models. J Comput Appl Math. 2010;234(7):2272–8.
76. Junge M, Brunner D, Becker J, Gaul L. Interface-reduction for the Craig-Bampton and Rubin method applied to FE-BE coupling with a large fluid-structure interface. Int J Numer Meth Eng. 2009;77(12):1731–52.
77. Fang M, Wang J, Li H. An adaptive numerical scheme based on the Craig-Bampton method for the dynamic analysis of tall buildings. Struct Des Tall Spec Build. 2018;27(1): e1410.
78. Thomas PV, ElSayed MSA, Walch D. Development of high fidelity reduced order hybrid stick model for aircraft dynamic aeroelasticity analysis. Aerosp Sci Technol. 2019;87:404–16.
79. Lim JH, Hwang DS, Kim KW, Lee GH, Kim JG. A coupled dynamic loads analysis of satellites with an enhanced Craig-Bampton approach. Aerosp Sci Technol. 2017;69:114–22.
80. Remedia M, Aglietti GS, Richardson G. A stochastic methodology for predictions of the environment created by multiple microvibration sources. J Sound Vib. 2015;344:138–57.
81. Goldman RL. Vibration analysis by dynamic partitioning. AIAA J. 1969;7(6):1152–4.
82. Fan Y, Zhou CW, Laine JP, Ichchou M, Li L. Model reduction schemes for the wave and finite element method using the free modes of a unit cell. Comput Struct. 2018;197:42–57.
83. Ning Y, Nan W, Xin Z, Wei L. Nonlinear flutter wind tunnel test and numerical analysis of folding fins with freeplay nonlinearities. Chin J Aeronaut. 2016;29(1):144–59.
84. Zhao Y, Jia XH, Zhang Y, Peng XY. Dynamic analysis of an offshore platform with compressor packages-application of the substructure method. J Offshore Mech Arctic Eng-Trans Asme. 2018;140(4): 041303.
85. Li H, Li G. Component mode synthesis approaches for quantum mechanical electrostatic analysis of nanoscale devices. J Comput Electron. 2011;10(3):300–13.
86. Chiello O, Sgard FC, Atalla N. On the use of a component mode synthesis technique to investigate the effects of elastic boundary conditions on the transmission loss of baffled plates. Comput Struct. 2003;81(28–29):2645–58.
87. Chen L, Xu YY, Sun LM. A component mode synthesis method for reduced-order modeling of cable networks in cable-stayed bridges. J Sound Vib. 2021;491: 115769.
88. Brizard D, Chiello O, Sinou JJ, Lorang X. Performances of some reduced bases for the stability analysis of a disc/pads system in sliding contact. J Sound Vib. 2011;330(4):703–20.

89. Voormeeren SN, van der Valk PLC, Rixen DJ. Generalized methodology for assembly and reduction of component models for dynamic substructuring. AIAA J. 2011;49(5):1010–20.
90. Jezequel L. A hybrid method of modal synthesis using vibration tests. J Sound Vib. 1985;100(2):191–210.
91. Jezequel L, Setio HD. Component modal synthesis methods based on hybrid models, Part II: numerical tests and experimental identification of hybrid models. J Appl Mech. 1994;61(1):109–16.
92. Qiu JB, Williams FW, Qiu RX. A new exact substructure method using mixed modes. J Sound Vib. 2003;266(4):737–57.
93. Ramsden JN, Stoker JR. Mass condensation: a semi-automatic method for reducing the size of vibration problems. Int J Numer Meth Eng. 1969;1(4):333–49.
94. Levy R, Guyan reduction solutions recycled for improved accuracy. in: NASTRAN User Experiences; NASA: 1971, p. 201–220.
95. Downs B. Accurate reduction of stiffness and mass matrices for vibration analysis and a rationale for selecting master degrees of freedom. J Mech Des. 1980;102(2):412–6.
96. Shah VN, Raymund M. Analytical selection of masters for the reduced eigenvalue problem. Int J Numer Meth Eng. 1982;18(1):89–98.
97. Golub GH, Van Loan CF. Matrix Computations. London, UK: North Oxford Academy; 1986.
98. Maia NMM, Silva JMM. Theoretical and experimental modal analysis. New York, USA: Wiley; 1997.
99. Li W. A degree selection method of matrix condensations for eigenvalue problems. J Sound Vib. 2003;259(2):409–25.
100. Henshell RD, Ong JH. Automatic masters for eigenvalue economization. Earthq Eng Struct Dynam. 1974;3(4):375–83.
101. Matta WK. Selection of degrees of freedom for dynamic analysis. J Press Vessel Technol. 1987;109(1):114.
102. Craig RR, Chang CJ. A review of substructure coupling methods for dynamic analysis. Adv Eng Sci. 1976;2:393–408.
103. Castanier MP, Tan YC, Pierre C. Characteristic constraint modes for component mode synthesis. AIAA J. 2001;39(6):1182–7.
104. Hong SK, Epureanu BI, Castanier MP. Next-generation parametric reduced-order models. Mech Syst Signal Process. 2013;37(1–2):403–21.
105. Aoyama Y, Yagawa G. Component mode synthesis for large-scale structural eigenanalysis. Comput Struct. 2001;79(6):605–15.
106. Kuether RJ, Allen MS, Hollkamp JJ. Modal substructuring of geometrically nonlinear finite-element models. AIAA J. 2016;54(2):691–702.
107. Mapa LDPP, das Neves FDA, Guimarães GP. Dynamic substructuring by the Craig–Bampton method applied to frames. J Vib Eng Technol. 2020;9(2):257–66.
108. Dickens JM, Nakagawa JM, Wittbrodt MJ. A critique of mode acceleration and modal truncation augmentation methods for modal response analysis. Comput Struct. 1997;62(6):985–98.
109. Qiu J-B, Ying Z-G, Yam LH. New modal synthesis technique using mixed modes. AIAA J. 1997;35(12):1869–75.
110. Ying Z, Qiu J. Exact residual modes and their synthesis techniques. J Vib Eng. 1996;9(1):38–46.
111. Ding Z, Li L, Hu YJ. A free interface component mode synthesis method for viscoelastically damped systems. J Sound Vib. 2016;365:199–215.
112. Bathe KJ, Ramaswamy S. An accelerated subspace iteration method. Comput Methods Appl Mech Eng. 1980;23(3):313–31.
113. Wilson EL, Itoh T. An eigensolution strategy for large systems. Comput Struct. 1983;16(1):259–65.
114. Zhao Q-C, Chen P, Peng W-B, Gong Y-C, Yuan M-W. Accelerated subspace iteration with aggressive shift. Comput Struct. 2007;85(19–20):1562–78.
115. Hasselman TK, Kaplan A. Dynamic analysis of large systems by complex mode synthesis. J Dyn Syst Meas Contr. 1974;96(3):327–33.
116. Craig RR, Chung Y-T. Generalized substructure coupling procedure for damped systems. AIAA J. 1982;20(3):442–4.
117. Craig RR, Ni Z. Component mode synthesis for model order reduction of nonclassically damped systems. J Guid Control Dyn. 1989;12(4):577–84.
118. Wang W, Kirkhope J. Complex component mode synthesis for damped systems. J Sound Vib. 1995;181(5):781–800.
119. de Kraker A, van Campen DH. Rubin's CMS reduction method for general state-space models. Comput Struct. 1996;58(3):597–606.
120. Muravyov A, Hutton SG. Component mode synthesis for nonclassically damped systems. AIAA J. 1996;34(8):1664–9.
121. Liu MH, Zheng GT. Improved component-mode synthesis for nonclassically damped systems. AIAA J. 2008;46(5):1160–8.
122. Kubomura K. Component mode synthesis for damped structures. AIAA J. 1987;25(5):740–5.
123. Xiang J, Ren G, Lu Q. Synthesis technique for the nonclassically damped structures using real schur vectors. AIAA J. 1999;37(5):660–2.
124. de Lima AMG, da Silva AR, Rade DA, Bouhaddi N. Component mode synthesis combining robust enriched Ritz approach for viscoelastically damped structures. Eng Struct. 2010;32(5):1479–88.
125. Touze C, Vizzaccaro A, Thomas O. Model order reduction methods for geometrically nonlinear structures: a review of nonlinear techniques. Nonlinear Dyn. 2021;105(2):1141–90.
126. Jain S, Tiso P, Rutzmoser JB, Rixen DJ. A quadratic manifold for model order reduction of nonlinear structural dynamics. Comput Struct. 2017;188:80–94.
127. Kuether RJ, Allen MS. A numerical approach to directly compute nonlinear normal modes of geometrically nonlinear finite element models. Mech Syst Signal Process. 2014;46(1):1–15.
128. Kerschen G, Peeters M, Golinval JC, Stephan C. Nonlinear modal analysis of a full-scale aircraft. J Aircr. 2013;50(5):1409–19.
129. Kuether RJ, Deaner BJ, Hollkamp JJ, Allen MS. Evaluation of geometrically nonlinear reduced-order models with nonlinear normal modes. AIAA J. 2015;53(11):3273–85.
130. Haller G, Ponsioen S. Nonlinear normal modes and spectral submanifolds: existence, uniqueness and use in model reduction. Nonlinear Dyn. 2016;86(3):1493–534.
131. Hollkamp JJ, Gordon RW, Spottswood SM. Nonlinear modal models for sonic fatigue response prediction: a comparison of methods. J Sound Vib. 2005;284(3–5):1145–63.
132. Frangi A, Gobat G. Reduced order modelling of the nonlinear stiffness in MEMS resonators. Int J Non-Linear Mech. 2019;116:211–8.
133. Haller G, Ponsioen S. Exact model reduction by a slow-fast decomposition of nonlinear mechanical systems. Nonlinear Dyn. 2017;90:617–47.
134. Shen YC, Vizzaccaro A, Kesmia N, Yu T, Salles L, Thomas O, et al. Comparison of reduction methods for finite element geometrically nonlinear beam structures. Vibration. 2021;4(1):175–204.
135. Rutzmoser JB, Rixen DJ, Tiso P, Jain S. Generalization of quadratic manifolds for reduced order modeling of nonlinear structural dynamics. Comput Struct. 2017;192:196–209.
136. Jain S, Tiso P. Simulation-free hyper-reduction for geometrically nonlinear structural dynamics: a quadratic manifold lifting approach. J Comput Nonlinear Dyn. 2018;13(7): 071003.
137. Vizzaccaro A, Salles L, Touze C. Comparison of nonlinear mappings for reduced-order modelling of vibrating structures: normal form theory and quadratic manifold method with modal derivatives. Nonlinear Dyn. 2021;103(4):3335–70.
138. Li MW, Jain S, Haller G. Nonlinear analysis of forced mechanical systems with internal resonance using spectral submanifolds, Part I: periodic response and forced response curve. Nonlinear Dyn. 2022;110(2):1005–43.
139. Li MW, Haller G. Nonlinear analysis of forced mechanical systems with internal resonance using spectral submanifolds,

Part II: bifurcation and quasi-periodic response. Nonlinear Dyn. 2022;110(2):1045–80.
140. Cenedese M, Axas J, Yang H, Eriten M, Haller G. Data-driven nonlinear model reduction to spectral submanifolds in mechanical systems. Philos Trans R Soc-Math Phys Eng Sci. 2022;380(2229):20210194.
141. Vizzaccaro A, Shen YC, Salles L, Blahos J, Touze C. Direct computation of nonlinear mapping via normal form for reduced-order models of finite element nonlinear structures. Comput Methods Appl Mech Eng. 2021;384: 113957.
142. Opreni A, Vizzaccaro A, Frangi A, Touze C. Model order reduction based on direct normal form: application to large finite element MEMS structures featuring internal resonance. Nonlinear Dyn. 2021;105(2):1272.
143. Li MW, Yan H, Wang L. Nonlinear model reduction for a cantilevered pipe conveying fluid: a system with asymmetric damping and stiffness matrices. Mech Syst Signal Process. 2023;188: 109993.
144. Jain S, Haller G. How to compute invariant manifolds and their reduced dynamics in high-dimensional finite element models. Nonlinear Dyn. 2022;107:1417–50.
145. El Mahmoudi A, Rixen DJ, Meyer CH. Comparison of different approaches to include connection elements into frequency-based substructuring. Exp Tech. 2020;44(4):425–33.